Redox Biology 56 (2022) 102448

Contents lists available at ScienceDirect

Redox Biology

journal homepage: www.elsevier.com/locate/redox

Simultaneous imaging of redox states in dystrophic neurites and microglia at Aβ plaques indicate lysosome accumulation not microglia correlate with increased oxidative stress

Stefan Wendt *, Sora Johnson, Nicholas L. Weilinger, Christopher Groten, Stefano Sorrentino, Jonathan Frew, Lucy Yang, Hyun B. Choi, Haakon B. Nygaard, Brian A. MacVicar **

Djavad Mowafaghian Centre for Brain Health, University of British Columbia, Vancouver, V6T 1Z3, Canada

ARTICLE INFO

Keywords:
Microglia
Alzheimer's disease
Oxidative stress
Neurodegeneration

ABSTRACT

The inter-relationship between microglia dynamics and oxidative stress (Ox-stress) in dystrophic neurites (DNs) at Alzheimer's Disease (AD) plaques may contribute to the pathological changes in neurons. We developed new *in vivo* imaging strategies to combine EGFP expression in microglia with neuronal expression of genetically encoded ratiometric redox sensors (rogRFP2 or roGFP1), and immunohistochemistry to investigate how microglia influence Ox-stress at amyloid plaques in 5xFAD AD mice. By simultaneously imaging microglia morphology and neuronal Ox-stress over time *in vivo* and in fixed brains we found that microglia preferentially enwrapped DNs exhibiting the greatest degree of Ox-stress. After microglia were partially depleted with the CSF1 receptor antagonist PLX3397, Ox-stress in DNs increased in a manner that was inversely correlated to the extent of coverage of the adjacent Aβ plaques by the remaining microglia. These data suggest that microglia do not create Ox-stress at Aβ plaques but instead create protective barriers around Aβ plaques possibly reducing the spread of Aβ. Intracranial injection of Aβ was sufficient to induce neuronal Ox-stress suggesting it to be the initial trigger of Ox-stress generation. Although Ox-stress is increased in DNs, neuronal survival is enhanced following microglia depletion indicating complex and multifactorial roles of microglia with both neurotoxic and neuroprotective components. Increased Ox-stress of DNs was correlated with higher LAMP1 and ubiquitin immunoreactivity supporting proposed mechanistic links between lysosomal accumulation in DNs and their intrinsic generation of Ox-stress. Our results suggest protective as well as neurotoxic roles for microglia at plaques and that the generation of Ox-stress of DNs could intrinsically be generated via lysosomal disruption rather than by microglia.

In Brief: Simultaneous imaging of microglia and neuronal Ox-stress revealed a double-edged role for microglia in 5xFAD mice. Plaque associated microglia were attracted to and enwrapped Aβ plaques as well as the most highly oxidized DNs. After partial depletion of microglia, DNs were larger with greater levels of Ox-stress. Despite increased Ox-stress after microglia removal neuronal survival improved. Greater Ox-stress was correlated with increased levels of LAMP1 and ubiquitin thereby linking lysosome accumulation and Ox-stress in DNs.

1. Introduction

Oxidative stress (Ox-stress) is a pathological hallmark of Alzheimer's Disease (AD) [1–3]. For example, post-mortem brain studies showed that markers of Ox-stress were significantly increased in brains from AD patients with dementia, but not in healthy controls nor in non-demented patients with amyloid neuropathology, indicating that Ox-stress is closely correlated with symptomatic AD [4]. In previous studies using

Abbreviations: AD, Alzheimer's Disease; Aβ, Amyloid beta; BACE1, Beta-secretase 1; DNs, Dystrophic neurites; GFAP, Glial fibrillary acidic protein; hSyn, human synapsin 1; IHC, Immunohistochemical; LAMP1, Lysosomal membrane protein 1; MAP2, Microtubule-associated protein 2; MPO, Myeloperoxidase; NEM, N-ethylmaleimide; NOX2, NADPH oxidase 2; Ox-stress, Oxidative stress; PFA, Paraformaldehyde; PLX, PLX3397; ROI, Region of interest; STED, Stimulated emission depletion; TREM2, Triggering receptor expressed on myeloid cells 2.

* Corresponding author.
** Corresponding author.
E-mail addresses: stefan.wendt@ubc.ca (S. Wendt), bmacvicar@brain.ubc.ca (B.A. MacVicar).

https://doi.org/10.1016/j.redox.2022.102448
Received 14 June 2022; Received in revised form 29 July 2022; Accepted 15 August 2022
Available online 20 August 2022

the genetically encoded redox indicator, roGFP1, the most intense Ox-stress in the brain was observed in the cellular elements termed dystrophic neurites (DNs) that cluster at amyloid beta (Aβ) plaques [5]. Long-term *in vivo* imaging also showed that Ox-stress in DNs at Aβ plaques preceded subsequent neuronal death [5]. DNs, first described by Oskar Fischer in 1907 [6] are swollen cellular structures that appear at Aβ plaques both in patients and in animal models of AD. DNs are abundant in vesicular and granular organelles [7,8] and are believed to be of axonal origin [9–14] with connections to viable neuronal cell bodies [14,15]. Microglia, the primary immune cells of the brain express many AD risk genes [16] and accumulate around Aβ plaques in human AD patients and in AD mouse models. They were found to closely associate with DNs in the brain of AD mice, but the functional role of this neuron-microglia interaction remains unknown [17]. The generation of Ox-stress and neuroinflammation at plaques has been hypothesized to be generated by Aβ acting on microglia [18,19] based on the expression of ROS generating enzymes in microglia, and reports that microglia secrete proinflammatory cytokines that induce Ox-stress in neurons [20]. Most recently it was suggested that microglia are the primary source of ROS in 5xFAD mice based on reduced inflammatory phenotypes of microglia *in vitro* by a small molecule which further ameliorates synaptic loss as well as reduced memory impairments [21]. However, a direct causal link between microglial activation and Ox-stress at Aβ plaques has not been demonstrated *in vivo*.

To investigate the relationship between microglia and DN Ox-stress at Aβ plaques, we developed a strategy to combine *in vivo* imaging of the new ratiometric redox sensor rogRFP2 [22] expressed in neurons with EGFP expression in microglia in 5xFAD AD mice. This allowed us to resolve relative degrees of Ox-stress in neurons at Aβ plaques *in vivo,* with simultaneous imaging of microglial morphology. In addition, we applied a new fixation technique that allowed us to preserve the oxidative state of roGFP1 to combine immunohistochemical (IHC) studies with *in vivo* imaging of neuronal Ox-stress. The ability to combine Ox-stress imaging with IHC allowed us to investigate the correlation of other potential stressors to the generation of Ox-stress at Aβ plaques, such as NOX2 activation, and test the impact of microglia depletion on the degree of neuronal Ox-stress. While microglia are tightly associated with highly oxidized DN, we find that, surprisingly, Ox-stress of DNs was increased after microglia depletion suggesting that microglia are not the primary source of ROS at plaques in aged mice but may instead have a neuroprotective function. Therefore we performed IHC imaging of other potential contributors to ROS generation at Aβ plaques to investigate their correlation with increased Ox-stress as a first step to evaluating their potential as candidates for generating Ox-stress when microglia are partially depleted [23,24]. Multiple sources of ROS may contribute to the AD pathogenesis at Aβ plaques independently of microglia. For example, Aβ itself can form ROS catalyzed by redox active metal ions [25]. Other proposed sources of neuronal Ox-stress in AD are ROS overproduction by dysfunctional mitochondria [26], and/or dysfunctional lysosomes that have been observed in DNs [27,28]. Redox levels in DNs were highly correlated with lysosome accumulation supporting suggestions they are principal contributors to Ox-stress in DNs.

2. Results

2.1. Tight associations between microglia and oxidized dystrophic neurites in vivo revealed by roGRFP2 imaging

We first established imaging strategies to simultaneously investigate neuronal redox states with rogRFP2 and microglial cells in acute brain slices prepared from 12 months old 5xFAD x CX3CR1-EGFP mice (see methods, Fig. S1). Neuronal rogRFP2 expression was induced by intracranial injection of AAV2/9-hSyn-rogRFP2. The promoter human synapsin 1(hSyn) was reported to be exclusively expressed in neurons and not glial cells [29]. This allowed us to image rogRFP2 redox levels in regions around Aβ plaques in 5xFAD x CX3CR1-EGFP mice to assess the extent of neuronal Ox-stress as well as the location and morphology of microglia. rogRFP2 expressing DNs can be readily found as swollen cellular structures surrounding Aβ plaques in these mice. A detailed description and illustration of rogRFP2 redox sensing properties are provided in the methods and Fig. S1. We used rogRFP2 because in addition to the green fluorescent redox sensing emission of roGFP2 it also displays a redox sensitive red fluorescent emission via ~50% FRET to the linked red fluorescent protein mApple (Fig. S1a) [22]. Therefore, due to these unique properties of rogRFP2 there are two ratiometric redox ratios at different emission wavelengths that are caused by the same two-photon excitation at 800 nm and 900 nm as illustrated in Fig. S1a. The images of the green and red fluorescent output are shown in Fig. S1b and are plotted in Fig. S1c. The green emission of the directly redox sensitive roGFP2 is labeled $R_{ox}F_{GFP}$ and the red emission from the mApple (that is excited by FRET from the redox sensitive roGFP2) is labeled $R_{ox}F_{RFP}$. rogRFP2 redox fluorescence is either displayed in pseudo colored green-red merged images (Fig. 1a, left panel) or by showing the calculated redox ratios as a spectrum (Fig. 1a, right panel).

We confirmed previous observations [5,27,28] that the swollen DNs around Aβ plaques in 5xFAD mice were round to slightly elongated with varying sizes and were much more oxidized than more distant neuronal processes (Fig. 1a, see arrows). We identified plaque associated microglia that only express EGFP in brain regions by digitally performing a raw pixel by pixel subtraction of rogRFP2 fluorescence from the images using FIJI channel subtraction (see methods). The structures expressing rogRFP2 were identified by the overlapping green and red emission (see methods and Fig. S1d). This approach was successful when EGFP expression was not brighter than rogRFP2 fluorescence to ensure successful channel subtraction (see methods). Using this technique, we found that highly oxidized DNs were often enwrapped by microglial cells in live tissue (Fig. 1b–c, arrow). To validate functional rogRFP2 expression in DNs, we bath applied DTT (5 mM, reducing agent) or diamide (2 mM, oxidizing agent) and detected commensurate shifts in rogRFP2 readouts (Fig. 1d), indicating DNs responded to cytosolic redox changes. Shifts in redox ratios were observed using $R_{ox}F_{RFP}$ (red emission: Em. 575–640 nm, Fig. 1d; for green emission and $R_{ox}F_{GFP}$ images see Fig. S2). Although DNs appeared to be severely oxidized, the application of diamide resulted in significantly greater oxidation ratios indicating that DNs were not fully oxidized. We further confirmed that the CX3CR1-EGFP positive cells express P2YR12 and Iba1 identifying them as microglia (Fig. S3). To further confirm that redox sensitivity is limited to rogRFP2 and not CX3CR1-EGFP we performed bath applications of DTT and diamide in mice with only CX3CR1-EGFP in microglia (i.e. no rogRFP2 expression) and found no shifts in fluorescence emissions of EGFP expressed in microglia using the rogRFP2 imaging settings (Fig. S4).

Functional rogRFP2 expression in DNs indicates that despite their swollen and peculiar morphology DNs are intact albeit unusual cellular structures. We further confirmed this by showing that DNs in acute brain slices of 12 months old mice do not take up propidium iodide, which labels dead cells (Figs. S5a–b). By performing patch-clamp experiments on DNs surrounding Aβ plaques we found that DNs had stable membrane potentials of ~-60 mV and displayed potassium as well as sodium currents (Figs. S5c–e) further confirming their functional properties and intact membranes.

The formation of Aβ plaques is correlated with a progressive increase in the number and size of oxidized DNs that develop over weeks to months [5]. To monitor the spatiotemporal interactions between microglia and neuronal Ox-stress during DN formation, we performed longitudinal imaging of plaques and surrounding DNs and microglia *in vivo*. Chronic cranial windows were implanted into 5xFAD x CX3CR1-EGFP mice injected with the AAV-rogRFP2 vector followed by bi-weekly imaging sessions (Fig. 1e). We employed our digital image subtraction strategy that we validated in brain slices to visualize microglia separately from DNs around Aβ plaques *in vivo* (Fig. 1f). Using our imaging parameters lipofuscin deposits that are commonly observed

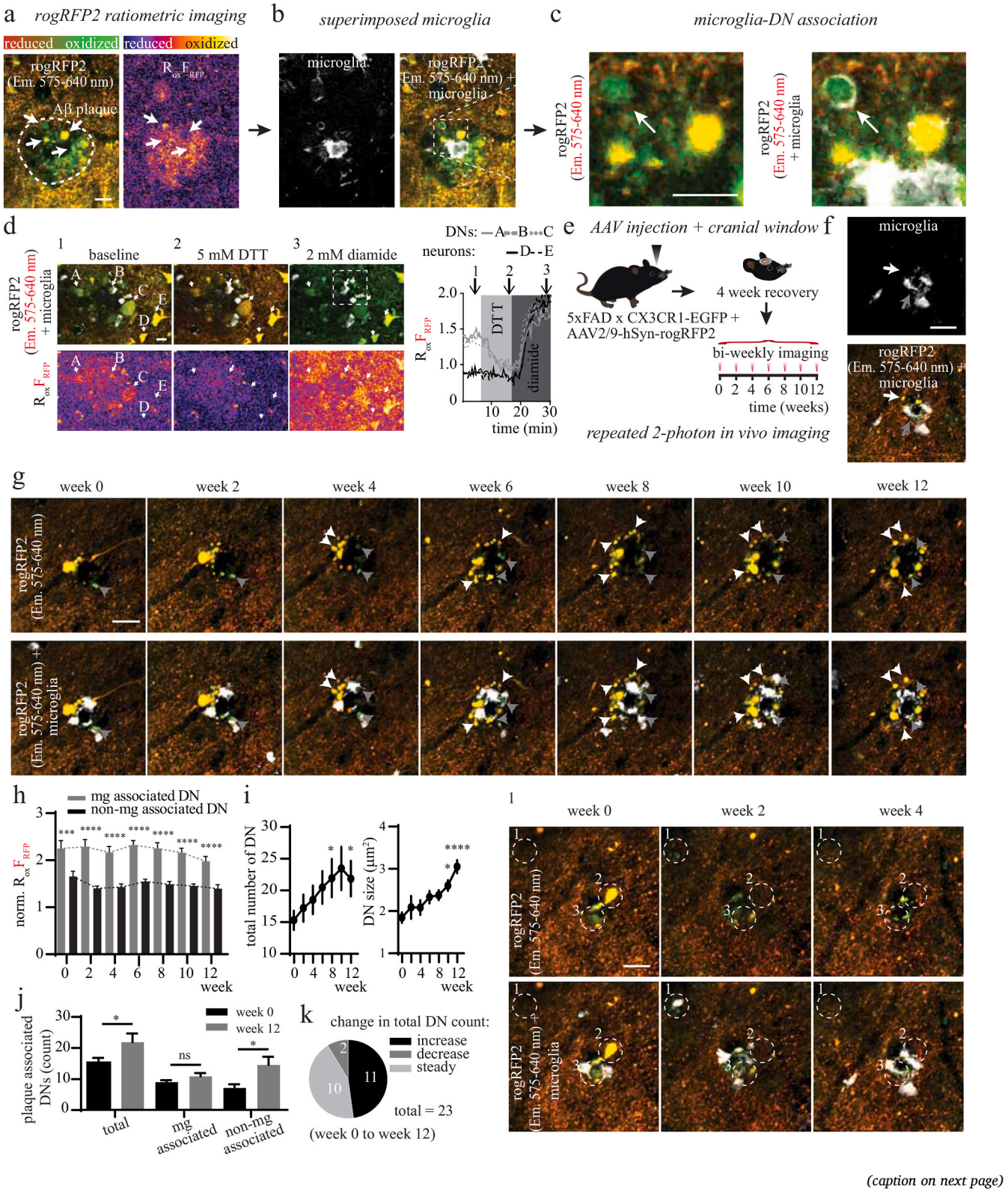

(caption on next page)

Fig. 1. Microglia closely associate with highly oxidized dystrophic neurites (DN) *in vivo* revealed by long-term *in vivo* imaging through a cranial window in rogRFP2 expressing 5xFAD x CX3CR1-EGFP mice. **a:** rogRFP2 expression in 5xFAD mice show increased oxidative stress in DNs (see arrows) around amyloid plaques displaying red rogRFP2 emission (Em. 575–640 nm). For green fluorescent rogRFP2 channels of this image see Fig. S1 **b:** Digitally subtracting from images the rogRFP2 red emission revealed green emission expressed in microglial cells around amyloid plaques and highly oxidized neurons surrounded by microglia (indicated by the arrow, see Fig. S1 for more details). Afterwards neuronal redox states can be quantified while considering the location of microglial cells. **c:** A microglial process (in white) is wrapping around an oxidized DN (rogRFP2 in green and red). In all subsequent micrographs microglia are shown in white and neuronal redox states in green-red. **d:** rogRFP2 expressed in acute brain slices of 5xFAD x CX3CR1-EGFP mice is functional shown by the changes in the redox ratios that were induced by DTT versus diamide applications. Regions of interests are labeled A-E (dystrophic neurites: A-C; surrounding neurons: D-E). **e**: A chronic cranial window was inserted into mice right after AAV injection and mice were allowed to recover for 4 weeks. Mice were then imaged bi-weekly for 3 months in 7 consecutive imaging sessions to follow plaque growths over time. **f:** Example of an identified plaque *in vivo*. Increased neuronal oxidation can be seen in the red emission channel (Em. 575–640 nm). Subtracting the red emission channels from the green emission reveals microglial cells around the plaque (see Fig. S2 for more details). A DN distant to a microglia is labeled with a white arrow while a neurite associated to a microglia is marked with a grey arrow. **g:** A series of images from the same plaque imaged over a period of 12 weeks is shown. DNs associated with microglia are labeled with a grey arrow while neurites distant to microglia are labeled with white arrows. **h:** At any given time point microglia associated DN are on average more oxidized than non-microglia associated DN. **i:** Averaged total number of DN increases over time on the left and increase in DN size over time on the right. Significance indicated using one-way ANOVA following Dunnett's test comparing all groups to week 0. **j:** Comparison of the average change in DN number between week 0 and week 12 in microglia associated and non-microglia associated DN reveals that the number of DN associated with microglia is constant and the increase in total DN numbers is due to non-microglia associated DN. **k:** Single plaque analysis of the change in total number of DN between week 0 to week 12 reveals that not all plaques are growing in DN numbers. **l:** Dynamic changes of DN [1–3] over time. 3 different DN and one microglia (*) are labeled as examples and 3 imaging time points are shown. White labelling indicates the structures are present whereas the red label indicates that the structures disappeared in subsequent imaging sessions. Note that a single microglia (*) and associated oxidized DN appeared together at one specific time point and were not detected before or after. Scale bars are 10 μm. (For interpretation of the references to color in this figure legend, the reader is referred to the Web version of this article.)

in older brains [30] were detected as very brightly autofluorescent puncta that were most pronounced in red emission [31] using 800 nm excitation and were excluded from analysis. We successfully followed 23 individual plaques from 3 mice, aged 8 to 9 months old, over 3-months. We identified DNs, quantified their rogRFP2 redox ratios and established whether microglia were associated with the DNs or not and tracked them over 7 imaging sessions (Fig. 1g). Redox levels were quantified in two groups of DNs defined as either associated with, or not associated with microglia (Fig. 1h). To account for changes in tissue optics at varying imaging depths, all redox ratios were normalized to redox levels from the surrounding neuropil. Interestingly, we found that DNs associated with microglia were substantially more oxidized throughout the entire imaging period (2.2-fold ± 0.6 vs. 1.48-fold ± 0.34, pooled data all timepoints, ****$p<0.0001$). In addition, the total number of observed DNs increased over time (week 0 to week 12, **$p < 0.01$, Fig. 1i) as well as their size (week 0 to week 10, *$p < 0.01$, week 0 to week 12, ****$p < 0.001$, Fig. 1i). This was attributed to an increase in DNs that were not associated with microglia (Fig. 1j). Over the 12-week observation period only 2 plaques showed decreasing number of DNs (Fig. 1k). We identified a subpopulation of persistent DNs that were trackable over several imaging sessions, and found location and presence of microglia to be extremely plastic with DNs and their location varying between imaging sessions. Three different regions of interest (ROI's) are marked in Fig. 1l, ROI 1 shows a region where both microglia and an oxidized DN were visible during only one imaging session indicating that they appeared and disappeared simultaneously. Conversely, ROI 2 shows a reduced DN which was not associated with microglia and disappeared after one imaging session. ROI 3 shows an oxidized DN surrounded by microglia which appeared to be removed or reduced in size in consecutive imaging sessions. This data suggests a highly dynamic turnover of DNs and their association with microglia which indicates that microglia could be mechanistically involved in 1) the formation of DNs around Aβ plaques 2) the generation of Ox-stress in DNs and 3) their removal from the brain.

2.2. roGFP1 redox sensing is preserved in PFA fixed brain tissue

To further evaluate DN Ox-stress around Aβ plaques and their interactions with microglia at high resolution we switched to imaging neuronal roGFP1 expression (exclusively green emission redox imaging) induced via intracranial injection of AAV2/9-CBA-roGFP1 to examine DN oxidation in APP/PS1 mice (*5*). As a first step we investigated the utility of immunohistochemical (IHC) staining after PFA fixation for identifying cell expression and in the second step we established a PFA fixation protocol that preserved the oxidative state of roGFP1 and was compatible with IHC staining. Staining for the neuronal marker microtubule-associated protein 2 (MAP2) revealed that only MAP2 positive neurons expressed roGFP1 (Fig. S6a) and that there was no overlap of roGFP1 with the microglial marker Iba1 or the NG2 cell marker Olig2. Although low levels of roGFP1 expression were observed in a subpopulation of GFAP-positive astrocytes (16 ± 5.6% of astrocytes), roGFP1 was predominantly expressed in neurons. Staining for PDGFRβ did not show any colocalization of roGFP1 expression with pericytes or cerebral blood vessels (Figs. S6b–e).

We developed and validated a strategy to preserve the redox state of roGFP1 by fixing tissue from 12 months old mice with 4% paraformaldehyde (PFA) supplemented with 20 mM N-ethylmaleimide (NEM) (see Fig. S1f). We established that supplementation with NEM during the fixation procedure in acute brain slices was both required and sufficient to preserve the redox levels at the time of fixation and prevented roGFP1 oxidation after fixation as previously reported [32,33] (see Fig. S7). At rest neuronal redox states appear almost fully reduced evident by the lack of an DTT effect (see Figs. S1c,e,g) and [22] which can only be preserved when using NEM during PFA fixation. In comparison after fixation without NEM neuronal somata redox states are almost twice as high without NEM ($R_{ox}F_{GFP}$ of 1.2 vs. 0.68, **$p<0.01$, 2-way ANOVA following Holm-Sidak test). Our data demonstrates that NEM supplementation provides remarkable preservation of neuronal redox states monitored by roGFP1 after tissue fixation. We believe that this is an underappreciated feature of roGFP1 and allows for quantitative in-depth analysis of Ox-stress in health and disease of the brain.

Based on our observations that redox measures from live neurons expressing roGFP1 were preserved after PFA fixation when NEM was also included, we hypothesized that PFA plus NEM fixed tissue could be an important tool to complement our *in vivo* imaging results for further investigations on Ox-stress in 5xFAD mice. These mice were perfused with 4% PFA and 20 mM NEM to fix the brain and preserve the roGFP1 oxidation state before sectioning. 2-photon imaging of roGFP1 expressing neurons and DNs around plaques in PFA and NEM fixed tissue revealed similar patterns of DN Ox-stress compared to our live *in vivo* observations. Using this approach, we were also able to compare levels of Ox-stress in different cortical regions. One hallmark of 5xFAD mice is that plaques form early in deep cortex layers (L5-6) while plaques in upper cortex layers (L1-2) form late and can only be found in aged mice [34]. Interestingly, DNs were significantly smaller in L1-2 compared to L5-6 while the level of Ox-stress was the same despite the difference in size (Fig. 2a). We then imaged slices from PFA and NEM perfused brains on a 1-photon confocal laser scanning microscope and found roGFP1

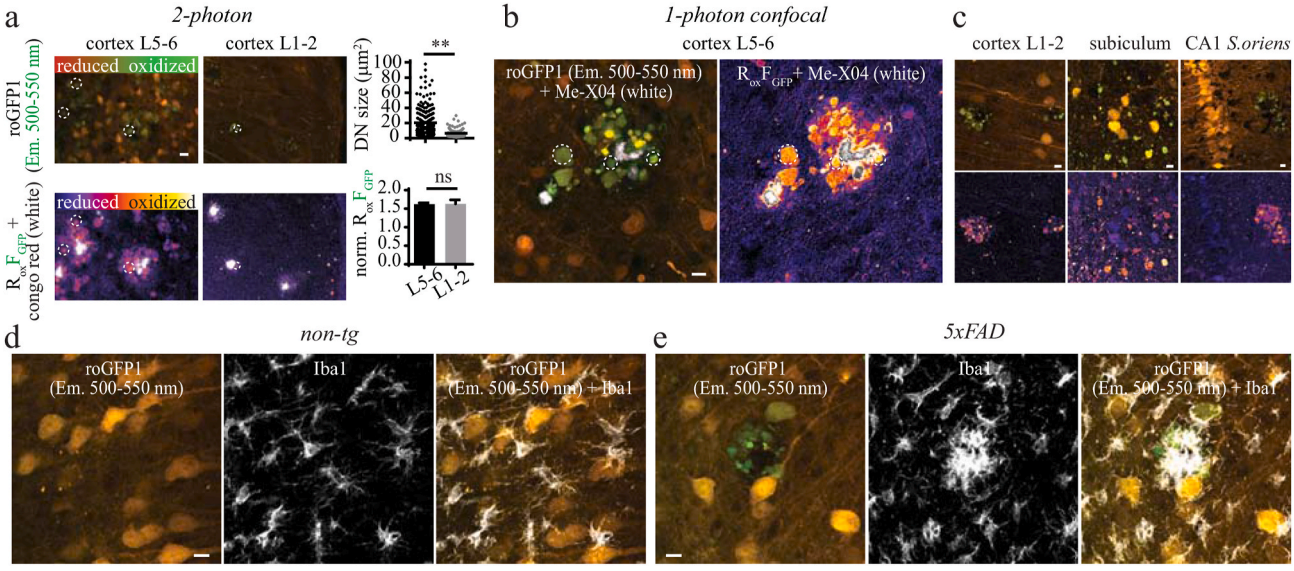

Fig. 2. Functional roGFP1 imaging (acquiring green fluorescence only, Em. 500–550 nm) in PFA perfused 5xFAD tissue confirms high levels of Ox-stress surrounding amyloid plaques. **a:** 5xFAD mice expressing roGF1P were perfused with 4% PFA +20 mM NEM, stored in PBS + NEM solution overnight and sliced into 120 µm thick slices afterwards. Plaques were stained with 20 µm congo red for 30 min prior to imaging. First, two different cortical regions were imaged, L1-2 or L5-6, on a 2-photon microscope. Increased redox ratios in DNs around amyloid plaques were well preserved. Exemplary DNs are marked by white circles. Sizes of DNs were significantly smaller in L1-2 compared to L5-6 (6.5 ± 2.4 vs. 20.5 ± 12.4 µm^2, N = 4 each, $^{**}p < 0.01$). Note that redox ratios of DN in both cortical regions did not differ. **b:** Slices were alternatively imaged on a confocal laser scanning microscope following a Methoxy-X04 staining revealing highly oxidized DNs surrounding dense amyloid plaques. Exemplary DNs are marked by white circles. **c:** Oxidative stress in multiple brain regions was confirmed including cortex, subiculum and the hippocampus. PFA perfused roGFP1 expressing brain tissue was immunolabelled for Iba1 to reveal location and morphology of microglia in non-tg (**d**) and 5xFAD (**e**) tissue. Scale bars are 10 µm. (For interpretation of the references to color in this figure legend, the reader is referred to the Web version of this article.)

oxidation states remarkably well preserved as evident by a higher dynamic range compared to live recordings (see methods). While we focused on cortical regions (Fig. 2b) this approach could be used to study Ox-stress in other brain regions of interest such as the subiculum or the hippocampus (Fig. 2c) where we also found high levels of Ox-stress.

2.3. Super resolution imaging confirms tight associations between microglia and oxidized DNs

Next, we sought to study spatial microglia-DN interactions in roGFP1 expressing PFA perfused 5xFAD brain tissue from 12 months old mice. Microglial cells were immunostained for Iba1 and imaged in parallel with roGFP1. This strategy allowed the analysis of the location and morphology of microglia in both non-tg (Fig. 2d) as well as 5xFAD mice (Fig. 2e). Note that the channel subtraction approach that we used for *in vivo* imaging of microglia in live mice with neurons expressing rogRFP2 and microglia expressing CX3CR1-EGFP was not applied in these experiments because only roGFP1 was used. In the experiments described here, roGFP1 ratios showing neuronal Ox-stress were preserved using PFA with NEM fixation and microglia imaging was possible only after immunofluorescence staining.

To further confirm the association between microglia and oxidized DNs, we stained for multiple microglia markers Iba1, cd11b and P2YR12 in PFA-fixed 5xFAD mouse tissue (Fig. 3a). Consistent with our *in vivo* findings from 5xFAD x CX3CR1-EGFP mice (Fig. 1), we found that microglia (identified by either of the 3 markers) were closely associated with DNs with their fine processes enwrapping or fully engulfing oxidized DNs. DNs were classified into two subpopulations based on their proximity to Iba1 stained microglia where a microglial associated DN is defined by a direct microglia-DN contact and alternately defined as non-microglia associated if no direct contact is observed by analyzing a given z-stack. Examples of DNs either strongly associated with microglia (examples labeled 1–4) or non-associated (examples labeled A-D) (Fig. 3b). Quantification of roGFP1 redox ratios from these distinct populations indicated that microglia preferentially associated with the most highly oxidized DNs ($+10.3 \pm 1.5\%$, $^{***}p < 0.001$, Fig. 3c–e).

Microglia processes are typically <2 µm with the finest filopodia <500 nm in diameter [35]. We therefore performed high-resolution stimulated emission depletion (STED) confocal imaging of Iba1 and roGFP1 in fixed 5xFAD brain slices to confirm the tight spatial association between microglia processes and oxidized DNs in fixed tissue (Fig. 3f). The microglia membrane stained by Iba1 revealed submicron DN-microglia associations. Importantly, microglia fine processes were clearly separated from the roGFP1 positive DNs suggesting that the DNs are not located within the microglial cytosol (see ROI1). Many oxidized DNs were observed using STED to be associated with microglial processes (Fig. 3f) or closely apposed to a microglial cell body (Fig. 3g).

To validate that the close interaction of microglia with DNs also occurs at plaques in AD patients, we performed immunofluorescence staining in human tissue from a sporadic as well as a familial AD patient. DNs are highly enriched with accumulated lysosomes and can be labeled with lysosomal membrane protein 1 (LAMP1) antibodies [28]. Staining for Iba1, LAMP1 and Aβ (Fig. S8) confirmed the spatial association between microglia and DNs in humans. In total, 13 plaques were analyzed and the total number of DNs per plaque was counted as well as the fraction of DNs closely associated with microglia (see arrows, Fig. S8). We found 4.9 ± 1 DNs per plaque of which 2.3 ± 0.6 DNs appeared closely associated with microglia (Fig. S8).

2.4. Treatment with PLX3397 reduced microglia numbers and neuron loss in 5xFAD mice without altering plaque load

Our observations of preferential association between microglia and highly oxidized DNs suggest that microglia proximity or contact may generate Ox-stress in DNs. To test this hypothesis, we depleted microglia from 5xFAD mouse brains by feeding mice with PLX3397 (PLX), a CSF1R antagonist [36–38] to determine how the degree of Ox-stress in DNs would change when microglia numbers were dramatically reduced. Neuronal roGFP1 expression was induced in mice (9 months age) via intracranially AAV injections as described in the methods. Mice were

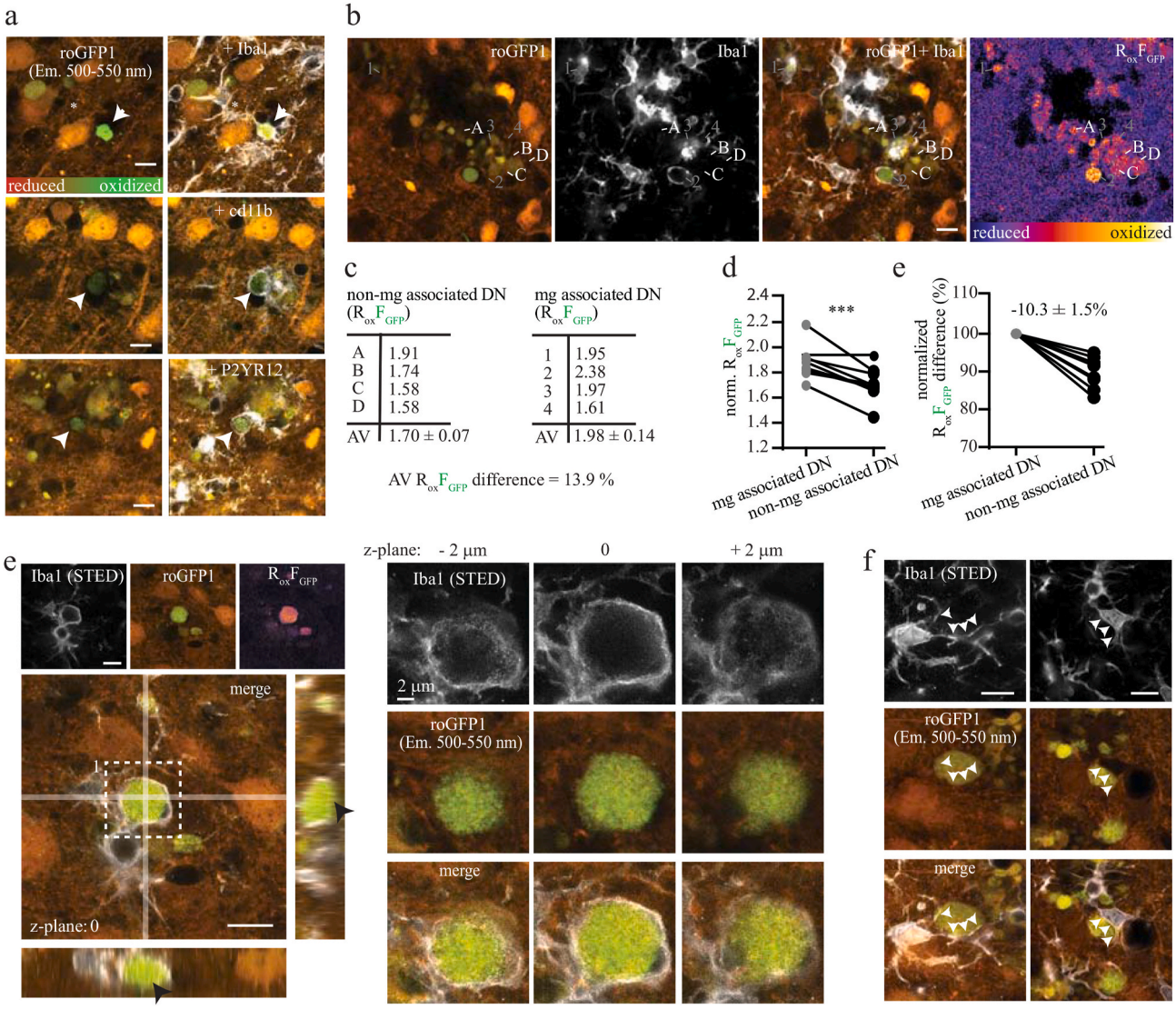

Fig. 3. The preferential association of microglia with highly oxidized DNs was confirmed by immunohistochemistry in PFA perfused roGFP1 expressing 5xFAD tissue. **a:** Staining for multiple microglia markers reveal how closely microglia associate with oxidized DNs in roGFP expressing 5xFAD tissue following confocal imaging using a 63X objective. A microglial soma (labeled with *) is seen in the upper panel with a process extending towards an enwrapped oxidized DNs (marked by arrow head). **b:** DNs surrounding plaques were manually separated into microglia associated (examples 1–4) and non-microglia associated (examples A-D) DNs. **c:** $R_{ox}F_{GFP}$ values in selected example DNs. On average, microglia associated DNs appear more oxidized. **d:** Quantification of $R_{ox}F_{GFP}$ in DNs in a larger sample size confirms more oxidized DNs when closely associated to microglia (1.88 ± 0.05 vs. 1.68 ± 0.04 $R_{ox}F_{GFP}$, N = 8 each, ***p<0.001, paired *t*-test). **e:** Normalizing each pair to microglia associated DN reveals a -10.3 ± 1.5% in a paired comparison. **f:** STED supported confocal microscopy using a 100X objective enables high resolution imaging of microglial engulfed oxidized DNs and microglia associated DNs. A 660 nm STED laser was used while imaging Iba1 (stained with Alexa Fluor 568) whereas roGFP1 was imaged without STED support. The image shows a microglial cell closely wrapping around a large highly oxidized DN (ROI 1). The DN in ROI 1 is almost fully wrapped by a microglial cell but does not appear to be within the microglial cytosol. The orthogonal view shows how the DN is not fully covered by Iba1 positive processes. **g**: Two example images show microglia closely associating with oxidized DNs without engulfing them. Microglia-DN contact area is indicated by arrows. Scale bars are 10 µm unless labeled otherwise.

maintained on chow either containing 290 mg/kg PLX to deplete microglia or matched control feed (Fig. 4a). After 8 weeks, mice were perfusion fixed as described above. We validated the efficiency of PLX treatment by immunostaining for Iba1 and found a ~60%–~80% depletion of microglia cells in 5xFAD and non-tg tissue, respectively (Fig. 4b). Quantification of Methoxy-X04 stained plaques revealed no significant impact of PLX on plaque load in 5xFAD mice (Fig. 4c).

Microglia depletion with PLX was previously reported to be neuroprotective with improved memory deficits in 5xFAD mice [36]. We confirmed these observations by examining neuronal death in cortex L5 of non-tg control and 5xFAD mice as well as PLX treated mice by DAPI and MAP2 immunohistochemical staining. MAP2 was detected in neuronal dendrites and somata but not in axons and DNs that lack MAP2 expression as previously reported [13] (Fig. 4d). By using MAP2 and DAPI we avoided counting DNs as false positive neuronal somata. Indeed, we found a substantial loss (49 ± 1.9 vs. 33 ± 2.3 $MAP2^+$ neurons per FOV, ****p<0.0001, 2-way ANOVA following Holm-Sidak test) of MAP2 positive neurons in 5xFAD mice which was reduced following PLX treatment (33 ± 2.3 vs. 39 ± 1.7 $MAP2^+$ neurons per FOV, *p<0.05, 2-way ANOVA following Holm-Sidak test).

2.5. Correlation of BACE1, Aβ, LAMP1 and ubiquitin immunoreactivity with Ox-stress in DNs

Beta-secretase 1 (BACE1), one of the major APP cleaving enzymes, is highly expressed in DNs and DNs are proposed to be sites of Aβ

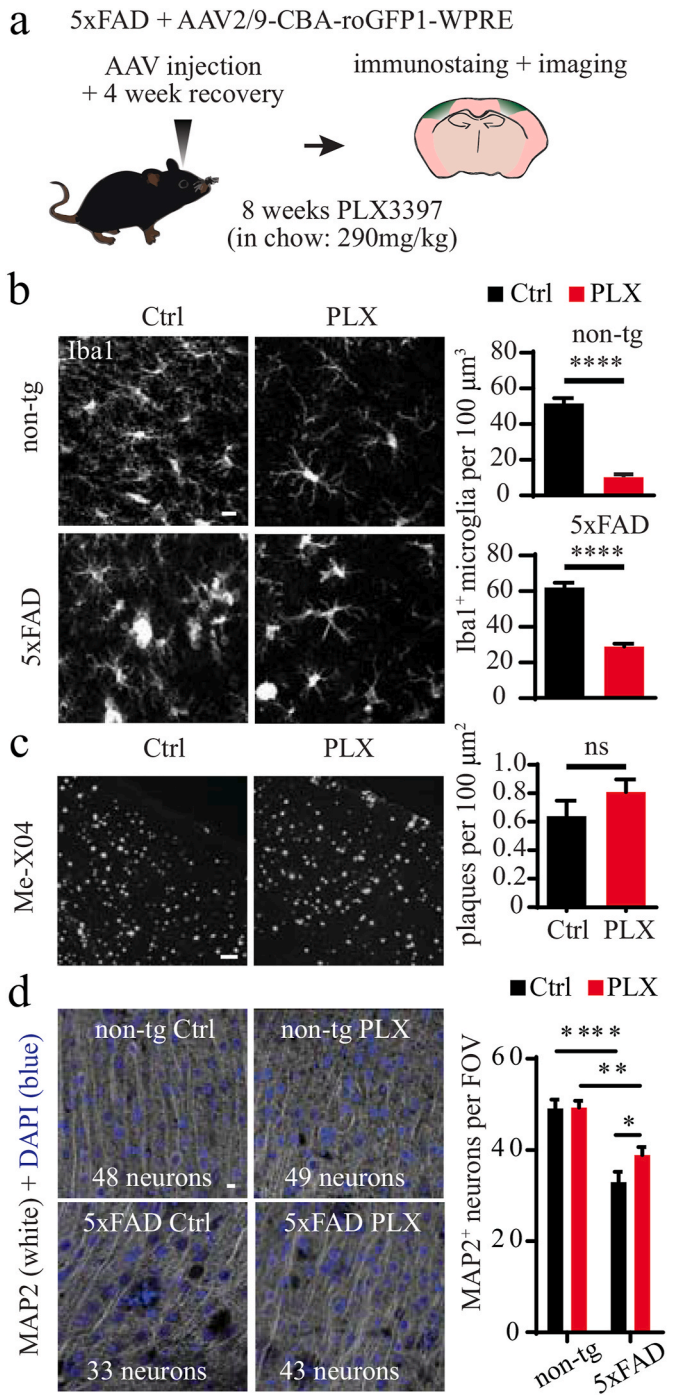

Fig. 4. PLX3397 (PLX) treatment efficiently depletes microglia while reducing neuron loss but does not alter plaque load in 5xFAD mice. **a:** 9 months old 5xFAD were injected with AAV2/9-CBA-roGFP1-WPRE before putting them on a PLX (290 mg/kg) diet for 8 weeks. Mice were perfused with 4% PFA +20 mM NEM afterwards. **b**: PLX treatment led to a robust reduction in microglia numbers in both non-tg and 5xFAD mice. **c:** PLX did not significantly change plaque load in 5xFAD mice. Slices were stained with Methoxy-X04 and cortical plaques were counted in slices from both control (N = 3 mice) and PLX (N = 4 mice) treated mice. **d**: Substantial neuron loss was found in 5xFAD control mice (49 ± 1.9 vs. 33 ± 2.3 $MAP2^+$ neurons per FOV, ****p<0.0001, 2-way ANOVA following Holm-Sidak test) and neuron loss was reduced when animals were treated with PLX (33 ± 2.3 vs. 39 ± 1.7 $MAP2^+$ neurons per FOV, *p<0.05, 2-way ANOVA following Holm-Sidak test). No significant difference was observed between control or PLX treated non-tg mice. Scale bars are 10 µm.

generation in the brain [13,14,39]. In addition, Aβ itself is posited to trigger Ox-stress in AD [25,40]. We investigated whether BACE1 – and APP/Aβ immunoreactivities were correlated with Ox-stress in DNs in 5xFAD mice to identify mechanisms of ROS generation. Surprisingly, we observed a negative correlation between BACE1 immunoreactivity and oxidation of DNs (Fig. 5a), with BACE1 levels highest in DNs with the lowest measures of Ox-stress (Fig. 5b, Correlations were tested using a linear regression fit following the Spearman test, ****$p < 0.0001$). Next, we stained for Aβ and APP (clone 6E10) around Aβ plaques and repeated the analysis comparing this staining with roGFP1 ratios (Fig. 5c). While 6E10 immunoreactivity (indicative of both Aβ and APP) was significantly increased in DNs compared to healthy appearing neuronal somata, we found Aβ/APP levels were highest in regions surrounding the DNs. A slight but significant increase in 6E10 expression with increasing levels of oxidation was found in DNs with a small but significant positive correlation with $R_{ox}F_{GFP}$ ratios (Spearman test: **$p < 0.01$).

Lysosome accumulation and increased expression of LAMP1 has been observed in DNs surrounding Aβ plaques in human and mouse models of AD [7,8,28]. DN lysosomes were reported to be dysfunctional and deficient of functional proteases [28]. Early stages of lysosomal dysfunction involve ubiquitination of lysosomes and permeabilization of the lysosomal membrane [41,42]. Lysosomes are highly oxidized at rest [43] suggesting they are a plausible ROS source leading to DN oxidation. We stained for LAMP1 in roGFP1 expressing 5xFAD tissue and found intense immunoreactivity for LAMP1 in DNs (Fig. 5e) with a highly significant positive correlation between LAMP1 levels and Ox-stress (Fig. 5f, Spearman test: ****$p < 0.0001$). In addition, co-staining for ubiquitin and LAMP1 (Fig. 5g) revealed that ubiquitin levels were increased in oxidized DNs (Fig. 5h, Spearman test: **$p < 0.01$) and that LAMP1 immunofluorescence was significantly correlated with ubiquitin in DNs (Fig. 5i, Spearman test: ****$p < 0.0001$). These data indicate that accumulation of dysfunctional and leaky lysosomes may be causally linked to ROS production because these lysosomal indicators were positively correlated with Ox-stress.

To further investigate potential sources of Ox-stress in DNs, we stained for two known ROS producing enzymes, myeloperoxidase (MPO) and NADPH oxidase 2 (NOX2), which were suggested to form ROS in AD [23,44–46]. Sparse and sporadic MPO staining was present in both microglia and DNs (Fig. S9a). MPO staining was never observed in GFAP positive astrocytes (Fig. S9b). Surprisingly, we did not find NOX2 expression in microglia or DNs surrounding amyloid plaques but did observe colocalization of NOX2 with GFAP positive astrocytes (Fig. S9c). Inhibition of NOX with apocynin (100 µM, 60 min) or MPO with MPO-I (100 µM, 60 min) in acute brain slices of roGFP1 expressing 5xFAD mice did not reduce Ox-stress in DNs in contrast to the significant reduction in Ox-stress by the positive control, a brief exposure to DTT (5 mM, 10 min). MPO and NOX2 do not appear to be significant sources for the profound Ox-stress observed in DNs surrounding Aβ plaques.

2.6. Insoluble Aβ aggregates following intracranial oligomeric Aβ injection drive Ox-stress in roGFP1 expressing non-tg mice

In the 5xFAD mouse model of severe amyloidosis and AD, the overproduction of Aβ1-42 is the key process triggering the AD pathology observed in these animals [34] suggesting that Aβ itself may also trigger the cascade that leads to Ox-stress in DNs surrounding plaques.

We tested the impact of directly injecting oligomeric forms of Aβ1-42 to determine if this would be sufficient to drive Ox-stress in non-tg animals expressing roGFP1. Instead of intracranial AAV delivery we used an AAV.php.eb-hSyn-roGFP1 construct that allowed retro-orbital delivery to generate extensive neuronal roGFP1 expression. This was followed with an intracranial Aβ injection a few weeks later and allowed us to avoid two consecutive intracranial surgeries in these mice (Fig. 6a). Oligomeric Aβ1-42 (oAβ, 350 µM, 2 µL, see WB for oAβ in Fig. 6a) was intracranially injected into one hemisphere into the somatosensory

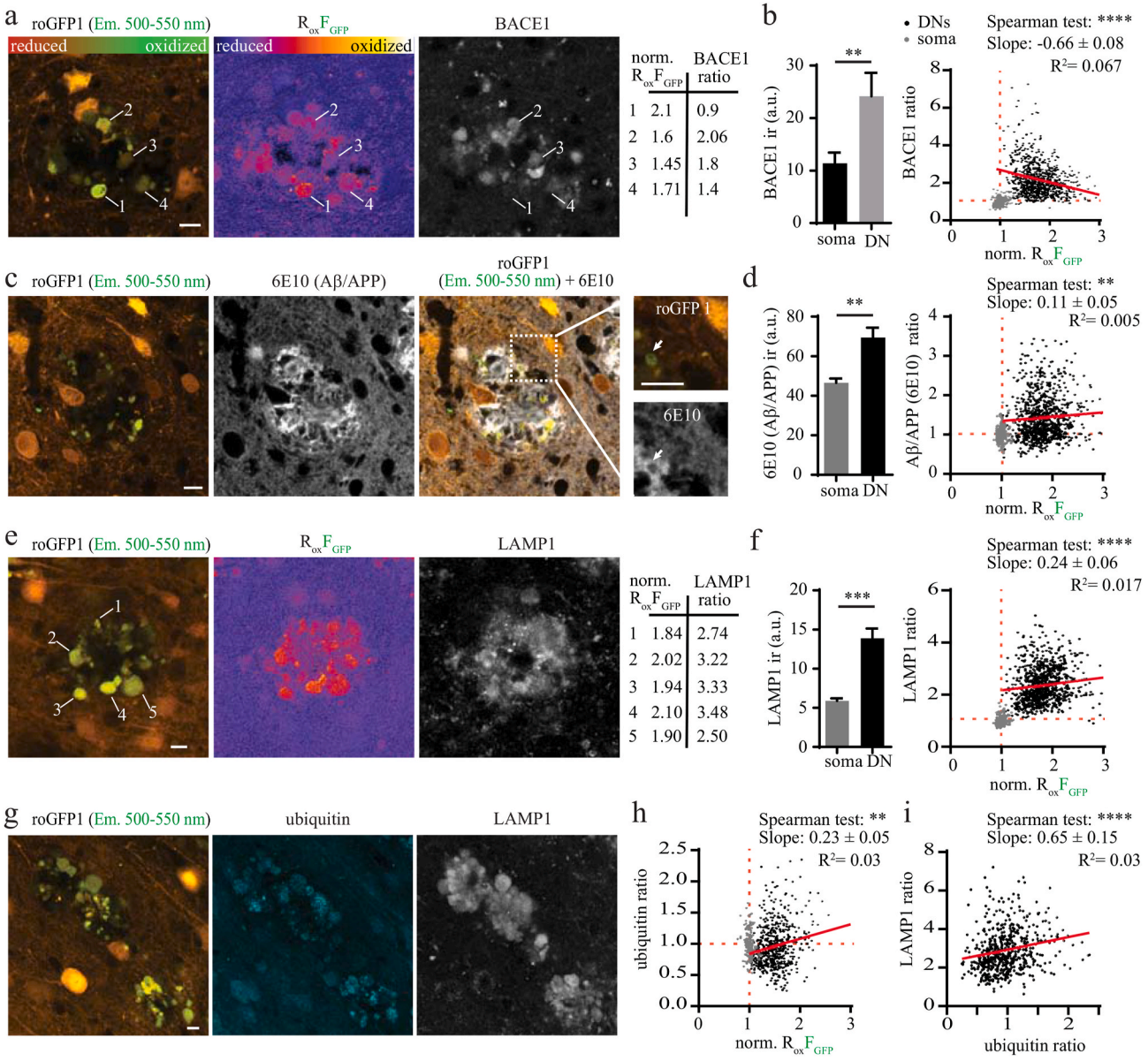

Fig. 5. Simultaneous roGFP1 and immunofluorescence imaging in PFA fixed 5xFAD brain tissue reveal high correlation of oxidative stress with lysosomal accumulation in dystrophic neurites. **a**: Staining for BACE1 and simultaneous imaging of roGFP1 reveals increased levels of BACE1 in oxidized DN. However, BACE1 immunoreactivity (ir) drops with most severe oxidative stress in DN (see arrows indicating example DN with varying levels of BACE1 and $R_{ox}F_{GFP}$). Quantification shown in **b**. **c:** Staining for 6E10, an antibody clone detecting APP and Aβ, shows increased levels in oxidized DN and most pronounced staining surrounding DN. Immunoreactivity of 6E10 does not decrease in most severe oxidized DN. Quantification shown in **d**. **e**: Staining for LAMP1 and simultaneous roGFP1 imaging (see arrows indicating example DN with varying levels of LAMP1 and $R_{ox}F_{GFP}$). f: LAMP1 immunoreactivity is significantly increased in DN. LAMP1 and redox ratios are highly significantly correlated suggesting that the amount of lysosome accumulation correlates with severity of oxidative stress in DN. **g**: Co-staining of ubiquitin and LAMP1 with simultaneous roGFP1 imaging showing high levels of ubiquitin and LAMP1 overlap. **h**: Ubiquitin expression is high throughout the tissue but increases significantly with more severe oxidation in DN similar to LAMP1 levels. **i**: Scatterplot of normalized LAMP1 and ubiquitin ratios reveals highly significant correlation. Scale bars are 10 μm.

cortex and scrambled Aβ1-42 (scAβ, 350 μM, 2 μL) was intracranially injected into the same region in the opposite hemisphere. Animals were PFA + NEM perfused, sliced, and imaged 7 days post-surgery.

Congo red staining (20 μM, 30 min) prior to 2-photon imaging allowed us to detect aggregated Aβ in the corpus callosum and layer 6 of the cortex exclusively in the oAβ injected hemisphere. Near these aggregates, we found that roGFP1 expressing neurons exhibited the swollen morphology of DNs (see arrows, Fig. 6b) with ratio changes consistent with enhanced Ox-stress. To confirm the congo red staining we next performed immunostainings using two different Aβ antibodies (clones 6E10 and mOC87) and found Ox-stress in close proximity to immunoreactive Aβ in the same brain regions (Fig. 6c). Immunostaining revealed more widespread distributions of Aβ than was observed using congo red (Fig. 6b). This may be due to the selective staining of aggregated Aβ by congo red versus all forms of Aβ by the antibodies.

2.7. Impact of microglia depletion on Ox-stress and LAMP1 levels in DNs

We quantified DN Ox-stress by imaging roGFP1 in perfusion-fixed brains (Fig. 7a) and co-stained for LAMP1 and microglia in PLX treated mice. roGFP1 measures of Ox-stress in DNs were higher after microglia depletion in PLX alongside an increase in DN size (Fig. 7b). Staining for Iba1 revealed that some microglia still present at plaques after PLX treatment were still closely associated with highly oxidized

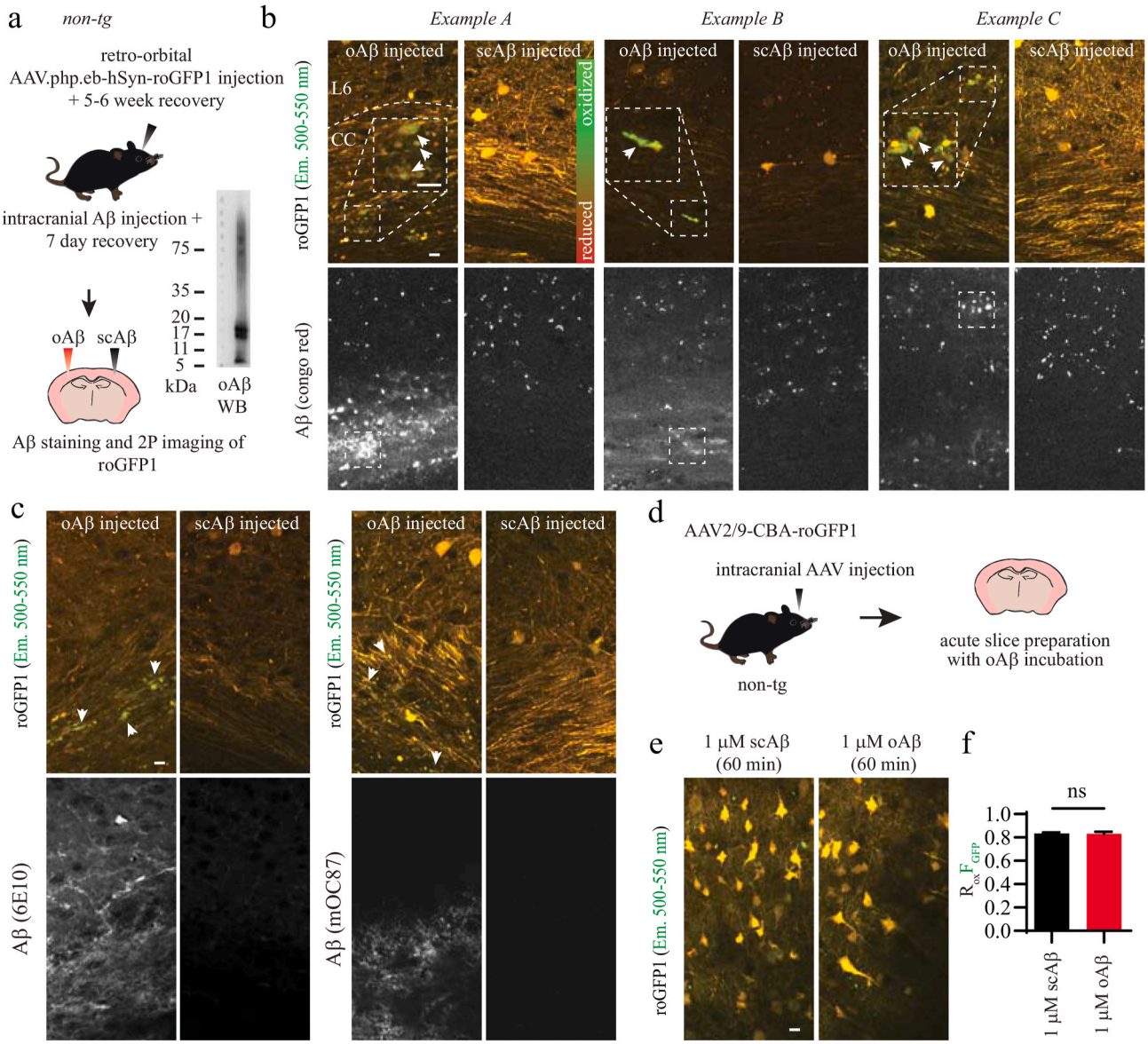

Fig. 6. Intracranial injection of oligomeric Aβ (oAβ) drives Ox-stress generation in non-tg C57BL/6 mice. **a:** Mice (4 total) were retro-orbitally injected with 3E11 gc of AAV.php.eb-hSyn-roGFP1 to induce brain-wide roGFP1 expression and allowed to recover for 5–6 weeks. Afterwards 2 µL 350 µM oAβ was injected into the left somatosensory cortex and 2 µL of scrambled Aβ1-42 (scAβ) into the right hemisphere. Mice were perfused, sliced and imaged 7 days post injection. Western blot for Aβ (6E10) confirming different sized oligomers after Aβ preparation. **b:** Brain slices containing the injection site on both hemispheres were stained with 20 µM congo red for 30 min and then imaged on a 2-photon microscope. Three examples from different animals are shown displaying congo red positive Aβ deposits in the deep cortex layer 6 (L6) or the corpus callosum (CC) with areas of high levels of Ox-stress in neuronal structures indicated by arrows revealed by roGFP1 imaging. **c:** Immunofluorescence staining for Aβ (either clone 6E10 or mOC87) confirmed the presence of Aβ and associated Ox-stress. Note that we found large areas of cortex and corpus callosum with obvious Aβ staining but the absence of Ox-stress (data not shown) using Aβ immunofluorescence indicating that Ox-stress only occurs close to the most aggregated forms of Aβ stained by congo red. **d:** Acute brain slices were prepared from roGFP1 expressing non-tg mice (following intracranial AAV injection as shown in previous figures, see Fig. S2) and incubated with either 1 µm oAβ or 1 µm scAβ for 60 min and then fixed with 4% PFA + 20 mM NEM. Imaging revealed that acute exposure to soluble oAβ is not sufficient to induce Ox-stress in neurons. Scale bars are 10 µm. (For interpretation of the references to color in this figure legend, the reader is referred to the Web version of this article.)

DNs as well as with the plaques themselves (Fig. 7c). Microglia have been proposed to form a protective barrier around amyloid plaque cores to protect surrounding tissue from Aβ toxicity [47]. We analyzed raw $R_{ox}F_{GFP}$ values as a function of distance to amyloid cores both in PLX and Ctrl treated 5xFAD by analyzing roGFP1 within a 40 µm radius of plaque cores (Fig. 7d). Quantification confirms the increased redox levels in PLX treated 5xFAD without normalization and, the comparison to non-tg cortex areas revealed that redox levels return to baseline level beyond a ~25 µm distance from plaque cores (Fig. 7e).

We found that oxidized DNs were more frequently observed outside the plaque environment in PLX treated 5xFAD mice (Fig. 7f, see arrows), suggesting enhanced Aβ toxicity around plaques in the absence of microglia triggering DNs formation.

If microglia play a neuroprotective role in AD by containing Aβ to plaque cores, then the extent of microglia coverage per plaque should be negatively correlated with Ox-stress in neighbouring DNs. The immediate peri-plaque area was defined by the presence of LAMP1 positive DNs surrounding a Methoxy-X04 positive plaque core (see methods) (Fig. 7f). The LAMP1 positive area, the sum of DNs surrounding the plaque core, was not significantly different between control and PLX treated mice whereas the microglial coverage per plaque was significantly lower in PLX treated mice (Fig. 7g). Reductions in microglia

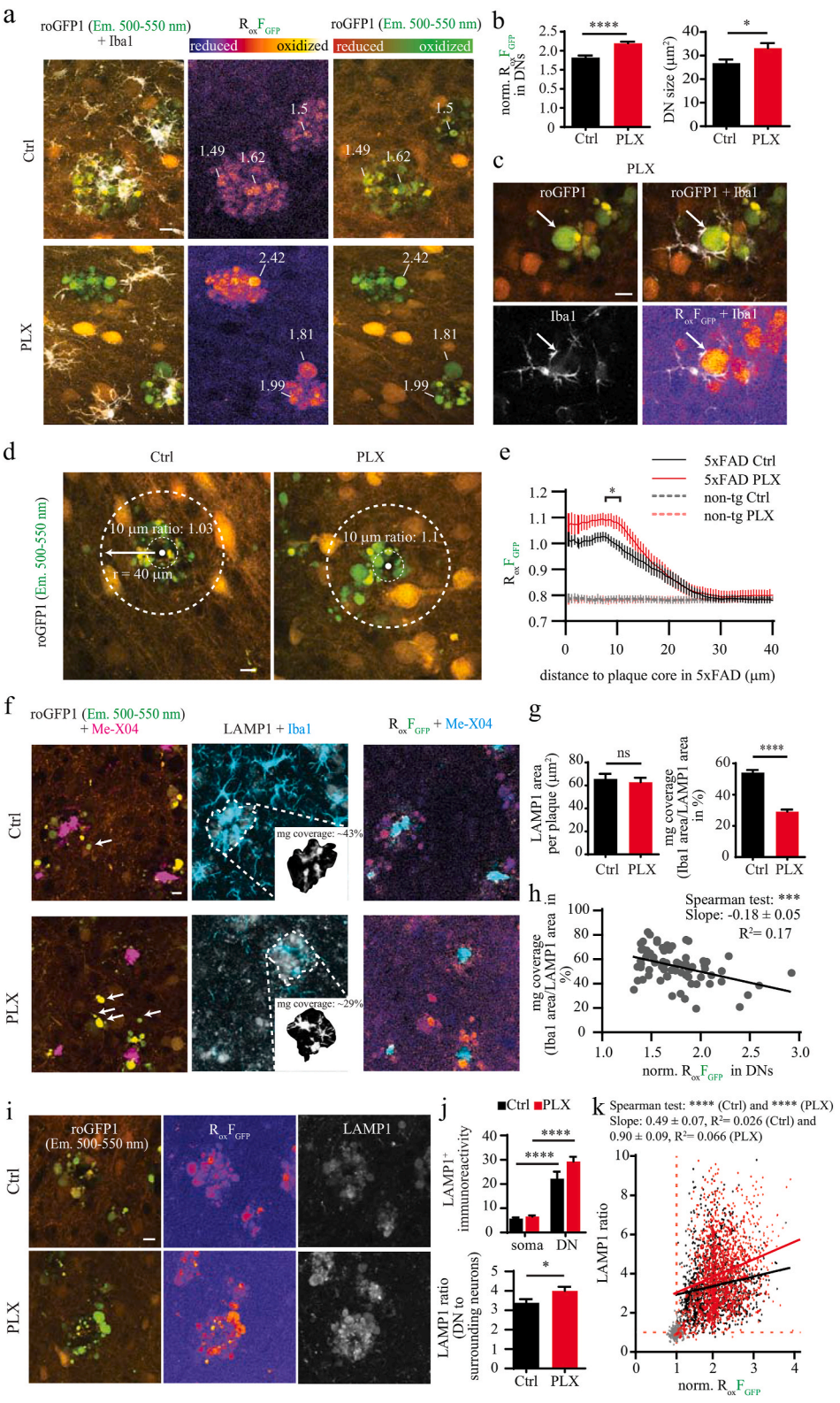

Fig. 7. Microglia depletion increases oxidative stress, LAMP1 levels and the size of DNs. **a**: Redox ratios of roGFP1 are increased in DNs in brain slices of PLX treated mice. Co-staining with Iba1 reveals location of microglial cells. Example $R_{ox}F_{GFP}$ values of representative DN are labeled. **b:** Quantification of normalized $R_{ox}F_{GFP}$ and average DN size in control and PLX treated mice. $R_{ox}F_{GFP}$ is increased from 1.82 ± 0.05 (N = 11) to 2.19 ± 0.04 (N = 12) (****p<0.0001, unpaired *t*-test) and the size of DN is increased from an average of 26.8 ± 1.6 (N = 10) to 33.2 ± 2.1 (N = 10) (*p<0.05, unpaired *t*-test). **c:** The surviving microglia in PLX treated mice still closely associate and engulf highly oxidized DNs. **d:** Raw $R_{ox}F_{GFP}$ values as a function of distance to plaque cores. Circular ROI's were drawn around plaques with a diameter of 40 µ. **e:** 5xFAD redox levels from PLX and Ctrl treated animals were compared to random areas in the cortex of non-tg mice. PLX redox levels are significantly higher than Ctrl levels in 5xFAD mice within 8–11 µm distance from the core (*p<0.05, two-way ANOVA following Tukey's test). Note that $R_{ox}F_{GFP}$ values do not differ from non-tg controls beyond a distance of ~25 µm to a plaque core. **f:** Co-staining of Methoxy-X04, Iba1 and LAMP1 in roGFP1 expressing 5xFAD tissue. Note that in PLX treated mice non-plaque associated oxidized DNs appear more frequent than in control 5xFAD mice (see arrows). Microglia coverage per individual plaque was quantified by masking the LAMP1 positive area surrounding a plaque (using z-projections of image stacks) and calculating the fraction of this area occupied by Iba1 positive microglia. **g**: Size of LAMP1 positive areas surrounding plaques does not differ between control and PLX treated 5xFAD whereas the microglia coverage is dramatically reduced in PLX treated mice. **h**: Microglia coverage and severity of Ox-stress in DNs inversely correlate. The fewer microglia are present in the immediate plaque-vicinity the higher the $R_{ox}F_{GFP}$ values in DNs. **i:** $R_{ox}F_{GFP}$ correlates with high LAMP1 immunoreactivity both in control and PLX treated animals. **j:** LAMP1 levels are significantly higher in PLX treated mice. **k:** In both groups LAMP1 ratios significantly correlate with increased Ox-stress. Scale bars are 10 µm.

plaque coverage were significantly correlated with increased severity of Ox-stress in DNs as indicated by the $R_{ox}F_{GFP}$ values of DNs (Fig. 7h, Spearman test: ***p < 0.001). This is consistent with a neuroprotective role for microglia to reduce Ox-stress by shielding the tissue around plaques from Aβ exposure. Finally, we examined the intensity of LAMP1 immunofluorescence and observed that LAMP1 immunoreactivity was significantly higher in microglia depleted mice after PLX treatment (Fig. 7i–j, *p = 0.035). LAMP1 immunoreactivity was well-correlated with oxidation severity in both PLX and control mice (Fig. 7k, Spearman tests: ****p<0.0001). These data further confirm our earlier observation that increased LAMP1 expression correlates with Ox-stress severity. However, we did not find significant differences in ubiquitin immunoreactivity between control and PLX treated 5xFAD mice (data not shown).

3. Discussion

Neuronal Ox-stress and microglial activation are known hallmarks of AD, yet the involvement of microglia in ROS generation leading to subsequent neuronal damage and memory loss is poorly understood. One reason for this is the lack of imaging strategies to study microglia and neuronal Ox-stress simultaneously. Here, we employed the 5xFAD mouse model of AD to study redox levels in the vicinity of Aβ plaques. Plaques in these mice first form at 6 weeks postnatal and continued amyloidosis leads to increased plaque loads with memory deficits and neuronal loss as early as 9 months of age [34,48]. We utilized new methods to simultaneously image neuronal redox states and microglial cells *in vivo*, in acute brain slices, and in PFA fixed tissue using the redox sensors rogRFP2 and roGFP1. Using these novel imaging strategies, we identified highly oxidized DNs surrounding Aβ plaques in 5xFAD mice. Our experimental approaches allowed us to examine the critical factors associated with the high level of Ox-stress in DNs. We found that microglia were preferentially associated with highly oxidized DNs. Surprisingly, removal of microglia from the brain exacerbated Ox-stress suggesting a neuroprotective role. However, depletion of microglia also rescued neuron loss confirming earlier reports [36]. The severity of Ox-stress in DNs correlates with the accumulation of lysosomes.

DNs surrounding amyloid plaques in APP/PS1 were reported to be highly oxidized using the redox sensor roGFP1 [5] and Ox-stress was hypothesized to subsequently lead to neuronal death. Microglia were found to closely associate with DNs [17] but the impact of microglia on Ox-stress in DNs was not previously investigated. A major obstacle for simultaneous neuronal redox and microglia imaging is that GFP expression, commonly used in microglia reporter mice, such as Csf1r-EGFP and CX3CR1-EGFP [49,50], does not allow for simultaneous imaging with roGFP redox sensors. Recently a variety of red fluorescent ratiometric redox sensors have been developed [51–53]. As an alternative approach, we employed rogRFP2, a next generation of a FRET-based roGFP-RFP fusion sensor [22,54] that allows for ratiometric redox imaging in both the green and red emission spectra. Expression of rogRFP2 in neurons of 5xFAD x CX3CR1-EGFP mice allowed us to simultaneously image microglia morphology as well as neuronal Ox-stress *in vivo*. Using repeated *in vivo* recordings of oxidized DNs and microglial cells, we found a dynamic turnover of DNs around plaques consistent with previous reports [15]. We conclude that microglia are attracted to highly oxidized DNs potentially triggering their removal by microglia.

To further understand ROS generation in DNs and microglia interaction, we investigated roGFP1 redox ratios in PFA fixed brain tissue, allowing us to perform immunostaining while preserving the redox states of roGFP1. Previous studies demonstrated preservation of roGFP1 redox signals after fixation in mice [33] and drosophila [32] when tissue fixation was combined with NEM which binds reactive thiol groups. Inclusion of NEM prevents future oxidation thereby locking roGFP in its oxidative state in the PFA fixed tissue. We successfully applied this technique in 5xFAD mouse brain slices to confirm the close interaction between microglia and severely oxidized DNs by staining for microglial marker proteins such as Iba1.

We initially hypothesized that microglia are the major source of ROS generation leading to Ox-stress in DNs and subsequent neuronal damage. Surprisingly, after depleting brain microglia in 5xFAD mice using PLX3397 [36,55], we observed an increase in DN oxidation and their physical size. We also confirmed that PLX3397 treatment reduced neuron loss in 5xFAD mice as previously described [36]. These data indicate that microglia are not the primary source of neuronal Ox-stress in DNs surrounding Aβ plaques and further suggest that neuroprotective as well as neurotoxic phenotypes of microglia act in parallel since removal of microglia also reduces neuronal loss and improves memory formation [36,37]. However, PLX induced depletion in younger (4 months) 5xFAD mice drastically reduced plaque formation in multiple brain regions, including cortex [55]. Recently, it was suggested that microglia produce ROS in 6 months old 5xFAD mice based on the observation that a small molecule reduces inflammatory phenotypes in microglia *in vitro* and further reduces synaptic loss, whole tissue redox stress and astrogliosis while improving memory function *in vivo* [21]. These apparent contradictions will guide future studies because they may arise due to the following reasons: 1. Our observations of Ox-stress using roGFP1 and rogRFP2 are limited to the immediate plaque environment and only to neuronal Ox-stress. We cannot exclude substantial Ox-stress in microglia and astrocytes which we would not detect with our method but could be detected with whole tissue assays. 2. The age of the mice was different (6 months [21] vs. 12 months in our study) and it is possible that microglia phenotypes vary substantially by age. 3. Multiple potential pathways of ROS generation exist in AD. 4. Our PLX treatment may have depleted a specific population of microglia with a distinct function regarding ROS generation different than the surviving microglia. 5. Microglia depletion might lead to increased infiltration of peripheral immune cells such as $CD3^{+}$/$CD8^{+}$ T-cells as shown in PLX5622 treated APP/PS1 mice [56]. The interaction of T-cells with the surviving population of microglia in the immediate plaque area could have impacted microglial ROS production leading to increased Ox-stress in DNs similar to reports of respiratory bursts of neutrophils after direct contact with activated T-cells [57] adding another potential layer of complexity.

Future experiments will test how earlier microglia depletion affects redox states in 5xFAD mice in different brain regions and what precise role non-microglial immune cells play in the generation of ROS in AD.

In contrast to a previous study in APP/PS1 mice [5] we normalized roGFP1 redox ratios of DNs to the redox ratios in surrounding healthy neurons or the neuropil. Changes in tissue transparency both *in vivo* and in fixed tissue preparations could have a significant impact on redox ratios. The rational for using this particular normalization was based on the following two observations: 1) The resting redox states of healthy neurons appeared to be fully reduced because there was no further changes in their baseline redox states when DTT was applied (Fig. S1c); 2) Ox-stress was predominantly limited to the direct vicinity of Aβ plaques and redox ratio values of neuronal cell bodies and the neuropil were similar to that of non-tg controls in areas distant to plaques (Fig. 7d–e). Note that the PLX induced increase in DNs Ox-stress was significant with and without normalization (Fig. 7b,e).

To further understand the underlying mechanisms of Ox-stress in DNs we imaged roGFP1 in parallel with immunostaining of putative contributors to ROS generation in 5xFAD tissue. We show that the initially high BACE1 activity declined as oxidation became more severe. The continued accumulation of Aβ in and around DNs suggests that Aβ itself is a likely player in generating Ox-stress around Aβ plaques of 5xFAD mice. To support this hypothesis, we investigated the impact of intracranial Aβ injection into the cortex of wild-type mice and found that Aβ alone was sufficient to induce Ox-stress in neurons. In addition, in the transgenic 5xFAD mice, we found a negative correlation between DN Ox-stress and microglia coverage around Aβ plaques. This suggests that microglia shield surrounding tissue from Aβ exposure as previously proposed by Condello et al. [47]. The formation of this 'microglia barrier' surrounding Aβ plaques was suggested to be neuroprotective evident by increased expression of protofibrillar Aβ-42 in subregions of plaques which were not covered by microglia which also correlated with increase in DNs in areas lacking microglia coverage [47]. This supports our hypothesis that a lack of microglia coverage leads to more Aβ exposure to DNs and subsequently is a plausible cause of increased Ox-stress. The discovery of mutations leading to partial loss of function of TREM2, a transmembrane receptor exclusively expressed in microglia in the brain, have highlighted neuroprotective functions of microglia in AD in recent years [58,59]. Loss of function in TREM2 was found to result in reduced numbers of microglia surrounding plaques and an almost complete loss of microglial encapsulation leading to increased severity of DN formation [60,61]. It was suggested that the neuroprotective effect of this microglial function stems from accelerated aggregation of Aβ rather than increased phagocytic activity [62].

We investigated the potential links between lysosomal dysfunction and DNs based on previous studies [12,27,28,63,64]. The accumulation of LAMP1 positive lysosomes was strongly correlated with Ox-stress severity in DNs (Fig. 5e–f). In addition, the lysosome enriched DNs were very immunopositive for ubiquitin (Fig. 5g–i) which could indicate the presence of dysfunctional lysosomes in these structures [41,42]. Based on previous reports that lysosomes are highly oxidized at rest [43], we hypothesize that membrane permeabilization in dysfunctional lysosomes [41] could be central to Ox-stress in DNs surrounding Aβ plaques. Most recently, lysosomal membrane permeabilization surrounding amyloid plaques was linked to neuron loss in 5xFAD mice [65]. In addition, lysosomal accumulation, and upregulation of lysosomal enzymes in oxidized DNs could also be a compensatory mechanism to counterbalance ROS as a key function for lysosomes is the degradation of dysfunctional organelles and proteins [66,67]. Microglia depletion with PLX led to higher LAMP1 levels in enlarged DNs. This increase in lysosomal numbers and lysosomal enzymes could be due to increased uptake and subsequent degradation of Aβ inside DNs due to reduced microglial coverage around plaques.

We propose that deciphering the causal relationship of lysosomal accumulation in either generating or responding to Ox-stress in DNs should be a key avenue for future research. Recent reports that Ox-stress only occurs in symptomatic AD patients but not in non-symptomatic patients with AD neuropathology [4] strongly underline the need to further understand the detailed underlying mechanisms of how Ox-stress is generated in AD.

Our observation that depleting microglia from the brain increased the degree of Ox-stress of DNs, suggests microglia may promote redox homeostasis of DNs. However, paradoxically neuronal death was also reduced illustrating the difficulties in attributing neuroprotective versus neurotoxic functions of microglial cells in AD [18,68,69]. When Ox-stress in DNs surrounding Aβ plaques was first reported the authors suggested that Ox-stress precedes a Caspase-3 dependent cell death pathway in neurons [5]. Since Ox-stress in DNs can persist for several weeks or even months it appears likely that a cell death pathway is not triggered immediately after Ox-stress occurs. We propose that Aβ is a key initial trigger for Ox-stress generation in DNs. The generation of DNs, and their subsequent lysosome accumulation, was suggested to occur due to Aβ induced dysfunction in the cytoskeleton of axons [14]. Furthermore, stabilizing microtubules was shown to reduce the number of DNs and to improve memory functions in AD mice [70,71]. Depletion of microglia might therefore increase Aβ exposure to neurons and subsequently exacerbate Ox-stress in DNs due to more cytoskeleton dysruptions and lysosome accumulation in our aged 5xFAD mice. Alternatively, microglia may acquire neurotoxic phenotypes in later stages of amyloidosis in AD and AD models [68,72] that could explain why the depletion of microglia reduces the loss of neurons in 5xFAD. This age dependent neurotoxic phenotype may ultimately overshadow the neuroprotective effects. Understanding the exact pathways of these underlying phenotypes will be a crucial aim for future studies to pharmacologically target microglial functions to both ameliorate Ox-stress and to reduce neuron death in AD.

4. Methods

4.1. Animals

All animal care protocols were approved by the University of British Columbia's Animal Care Committee in compliance with the Canadian Council on Animal Care guidelines. 5xFAD mice [34] were either crossbred with C57BL/6 mice (experiments using roGFP1) or crossbred with CX3CR1-EGFP mice (experiments using rogRFP2). Mice were kept under a 12h dark/light cycle with food and water supply *ad libitum*.

4.2. Intracranial AAV injections

To induce neuronal expression of either roGFP1 or rogRFP2 we performed intracranial AAV deliveries into the cortex of adult mice. Mice used for live *in vivo* recordings were 32–34 weeks old whereas all other mice were 40–44 weeks old. Animals were anesthetised with 1–3% isoflurane before and throughout the surgery and transferred to a stereotactic frame. Briefly, a small hole was drilled above the somatosensory cortex and 1–2 μL of AAV solution (either AAV2/9-CBA-roGFP1 or AAV2/9-hSyn-rogRFP2) was injected 1 mm deep into the cortex using a glass micropipette and a Hamilton syringe. All mice were allowed to recover for 4 weeks prior to experiments.

4.3. Retro-orbital AAV injection

To induce brain-wide roGFP1 expression without the need of a surgery for intracranial delivery we performed retro-orbital injections [73] of a AAV.php.eb.-hSyn-roGFP1 construct into non-transgenic C57BL/6 mice. In brief, mice were briefly anesthetized with 2% isoflurane and up to 150 μL of AAV solution (diluted with saline to a titer of 3E11 gc) were slowly injected behind the right eye. Afterwards animals were allowed to recover for 5–6 weeks.

4.4. Oligomeric Aβ preparation

Synthetic Aβ1-42 was purchased from ERI Amyloid Laboratory (Oxford, USA). Lyophilized powder was used to prepare oligomeric Aβ. In brief, 40 μL DMSO was added to 500 μg Aβ and thoroughly mixed. After 20 min, 2 mL of Ham's F12 media was added and the solution was left at room temperature over night. The solution was centrifuged using a 3K cutoff filter (UFC5003, Millipore) at 14,000g for 15 min. Afterwards the solution was washed and centrifuged twice again with PBS (14,000g for 15 min). Finally, the filter was flipped and spun down at 1,000g for 2 min to collect the oligomeric Aβ (oAβ).

4.5. Acute brain slice preparations and recordings

Mice were anesthetized with 5% isoflurane prior to decapitation. Brains were rapidly removed and placed into ice-cold slicing solution containing (in mM): NMDG, 120; KCl, 2.5; $NaHCO_3$, 25; $CaCl_2$, 1; $MgCl_2$, 7 NaH_2PO_4, 124; glucose 20; sodium pyruvate. 2.4; sodium ascorbate, 1.3. The solution was saturated with carbogen (95% O_2/5% CO_2) with a pH of 7.4. Coronal brain slices (250 μm) were prepared using a vibratome (VT1200, Leica, Nussloch, Germany) and stored at room temperature in artificial cerebrospinal fluid (ACSF) containing (in mM) for a maximum of 4 h: NaCl, 126; KCl, 2.5; $NaHCO_3$, 26; $CaCl_2$, 2; $MgCl_2$ 2, 7; NaH_2PO_4, 1.25; glucose, 20. Solution was saturated with carbogen and set to a pH of 7.4. Brain slices were transferred to a 2-photon laser scanning microscope and continuously perfused with the same ACSF at room temperature. For assessing acute cell death, 20 μm propidium iodide (PI) was washed in via the perfusion pump and cells filling up with bright red fluorescent PI were considered dead. The Myeloperoxidase Inhibitor-1 (MPO-1, Sigma Aldrich) and apocynin (Sigma Aldrich) were both used at a concentration of 100 μm and acute brain slices were incubated for 60 min in a static chamber saturated with carbogen.

4.6. Acute neuronal redox imaging using rogRFP2

We developed an *in vivo* strategy for simultaneously imaging neuronal redox states and microglia in order to study the spatial-temporal dynamics of microglia interactions with oxidized DNs around plaques in the 5xFAD mouse model of AD. This involved expressing in 5xFAD x CX3CR1-EGFP transgenic mice, the recently developed rogRFP2, a second-generation FRET based fusion ratiometric redox sensor. The rogRFP2 FRET sensor is a fusion of roGFP2 with the red fluorescent protein mApple [22,54]. The reduction-oxidation

sensitive protein roGFP2 is the redox sensing part of the construct, linked to mApple via a fixed length amino acid sequence, and serves as an excitation ratiometric sensor [74,75]. roGFP (both roGFP1 and roGFP2) contains specific insertions of cysteines in close proximity to the fluorophore which allow for the formation of disulfide bonds upon protein oxidation. Disulfide bond formation shifts the excitation maximum to a lower wavelength (excited with ~800 nm for 2-photon imaging) while the excitation properties of reduced roGFP is closer to native GFP (excited with ~900 nm for 2-photon imaging). However, the roGFP emission spectrum is not altered by its oxidation state. Thus, rogRFP2 is alternately excited by 800 and 900 nm to allow for time series or z-stack recordings (for 2-photon imaging, channel I and II respectively) and the green fluorescence (Em. 500–550 nm) is acquired for both channels. The advantage of rogRFP2 is that the green fluorescence emission of roGFP2 generates red fluorescence (Em. 575–640 nm) emission from mApple via FRET transfer of ~50% of the redox sensitive green emission of roGFP2 [22]. The emission is acquired for both excitation wavelengths (channel III and IV). Since the two proteins are linked via a fixed spatial distance the redox sensitive green emission is transferred into a ratiometric red emission. This has the advantage of expanding the redox sensing properties to the red emission spectrum (Fig. S1a) and allows analysis of the EGFP-microglia that only exhibit green fluorescence but do not show the overlapping red fluorescence that occurs with rogRFP2.

First, functional neuronal expression of rogRFP2 was validated by injecting AAV2/9-hSyn-rogRFP2 (2 μL each hemisphere, somatosensory cortex, 1 mm deep) into C57BL/6 mice following 2-photon imaging in acute brain slices 4 weeks post-injection. After stable redox ratios were observed in rogRFP2 expressing neurons, the intracellular oxidizing agent diamide (2 mM) was bath applied following by washout and superfusion with the reducing agent dithiothreitol (DTT, 5 mM). This progressive bath application of diamide followed by DTT demonstrated that rogRFP2 ratios in expressing neurons and dendrites were modified by reducing and oxidizing agents thereby validating functional expression (Fig. S1c). For every time frame of the recording a redox ratio was quantified for both the green ($R_{OX}F_{GFP}$, dividing channel I by II) and red emission ($R_{OX}F_{RFP}$, dividing channel III by IV) of rogRFP2. As reported earlier, rogRFP2 dynamic range is lower in the red emission channel due to incomplete FRET and contamination of intrinsic redox-insensitive mApple fluorescence [22] (Fig. S1c). We confirmed that only green and red emission of rogRFP2 in DNs and neurons (but not EGFP in microglia, see also Fig. S4) were sensitive to DTT or diamide by analysing redox changes in DNs associated with microglia. Shifts in rogRFP2 were only detected in DNs with no measurable changes in EGFP-expressing microglia (Fig. S1e). These data confirm that EGFP emission from microglia can separated from rogRFP2 in CX3CR1-EGFP mice and be used for morphological analysis (Fig. S1d).

4.7. Simultaneous microglia and neuronal redox imaging in live tissue

Our goal was to take advantage of the ratiometric red fluorescent properties of rogRFP2 by using the sensor in 5xFAD x CX3CR1-EGFP mice. Microglia in these mice exhibit only green fluorescence whereas rogRFP2 expressing neurons exhibit both green and red fluorescence with this dual excitation at 800 and 900 nm. Therefore, post-hoc analysis entailing the digital subtraction of the red emission from the green emission channel removed signals from neurons and allowed us to observe the microglial-specific green fluorescence to reveal their location and morphology in the tissue with respect to neurons expressing the redox sensor (Fig. S1d). The fluorescence intensity values of both red emission channels (III and IV) were combined and added together by raw channel addition using FIJI (in order to cover both oxidized and reduced neuronal rogRFP2) and subsequently subtracted from green emission channel II. Channel II was chosen for this because microglial EGFP emission is much brighter using 900 nm instead of 800 nm excitation wavelengths and therefore offers much better channel subtraction results. To avoid any potential contamination of neuronal Ox-stress by microglial EGFP fluorescence, we chose to restrict our rogRFP2 analysis to the red fluorescence spectrum and $R_{ox}F_{RFP}$. Note that for the channel subtraction to effectively reveal microglial morphology the rogRFP2 expression and brightness can not exceed microglial EGFP expression. Therefore, we carefully selected regions in the cortex in which rogRFP2 fluorescence intensities were similar to EGFP. In future studies the use of a red fluorescent microglia reporter mouse in conjunction with roGFP1 would be useful for separating microglial morphology from neuronal Ox-stress.

4.8. Long-term in vivo imaging

After the AAV-rogRFP2 vector was injected into 5xFAD x CX3CR1-EGFP mice chronic cranial windows (4 mm diameter) were inserted during the same surgery.

Mice were allowed to recover for 4 weeks before 7 consecutive bi-weekly 2-photon imaging sessions were conducted. The first imaging time point was defined as week 0 whereas the last one as week 12. Plaques in cortex L1-2 were identified by the presence of oxidized dystrophic neurites around a dark plaque core and the coordinates were saved and used to relocate the same region in following imaging sessions.

4.9. Electrophysiology

Electrophysiology experiments on DNs were performed on acute cortical slices from 5xFAD mice transfected with the AAV roGFP1 construct. After stabilization, slices were transferred to a recording chamber perfused with ACSF (33°C, stage heater from Luigs and Neumann). DNs were visually identified using transmitted IR illumination, and roGFP1 images were captured prior to whole-cell patch clamping to confirm the redox ratio. Whole-cell patch clamp recordings were obtained using thin-walled borosilicate glass electrodes (Warner) pulled to a fine tip resistance of 6–8 MΩ (P-97 Flaming/Brown Micropipette Puller, Sutter Instrument) for patching small neurites. Electrodes were filled with intracellular recording solution, consisting of (in mM): 108 K-Gluconate, 3 KCl, 2 $MgCl_2$, 8 Na-Gluconate, 1 K_2-EGTA, 0.23 $CaCl_2$, 4 K_2-ATP and 0.3 Na_3-GTP at pH 7.25 with 10 HEPES. The inert dye Alexa Fluor 594 (100 μM, ThermoFisher) was included in the intracellular solutions to fill and visualize patched DNs. Recordings were made using a MultiClamp 700B amplifier and a Digidata 1440A digitizer controlled using Clampex 10.7 software (all from Axon Instruments, Molecular Devices). Current-voltage relationship experiments were conducted at a holding potential V_m = -60 mV, with +5 mV steps (200 ms) starting at -80 mV. For current clamp recordings, 2–5 pA episodic current injections were performed to probe for action potential firing. All data were analyzed in Clampfit 10.7 (Axon Instruments, Molecular Devices).

4.10. Cardiac perfusions

To perform redox imaging and immunofluorescence staining in mice expressing roGFP1 we transcardially perfused 12 months old non-tg and 5xFAD mice with 4% paraformaldehyde (PFA) supplemented with 20 mM NEM to preserve the redox state of roGFP1. In short, mice were intraperitoneally injected with an overdose of urethane following a thoracotomy. A needle was inserted into the heart angled via the left ventricle towards the aorta. The right atrium was cut and 15 ml of PBS +20 mM NEM was perfused through the needle. Afterwards 35 mL of PFA + NEM solution was perfused and the brains were dissected and stored in the same solution over night before 120 μm thick brain slices were prepared and subsequently stored in a cryoprotective solution (CPS) containing (for 1 L): Sucrose, 300g; PVP-40, 10g; 0.1 M phosphate buffer, 500 mL; ethylene glycol, 300 mL; NEM, 20 mM.

4.11. Western blot

Oligomeric Aβ was heated at 95°C for 5 min in Laemmli Sample buffer under reducing conditions (5% β-mercaptoethanol) before loading onto gels. Gels were transferred to 0.2 μm pore-size polyvinyldene fluoride (PVDF) membrane using a Trans-Blot Turbo semi-dry transfer system (Bio-Rad). Blocking and antibody incubations took place in blocking buffer (5% skim milk in TBS with 0.1% Tween 20). Primary antibody used was: 1: 1000 (6E10, Biolegend, San Diego, US). Secondary antibody used was: 1: 2000 horseradish peroxidase (HRP)-conjugated donkey anti-mouse (Jackson Immunoresearch). Blots were imaged using a C-DiGit Western blot scanner (LI-COR)

4.12. Intracranial Aβ injections

The protocol for stereotactic Aβ injections was adapted from Ref. [76]. Non-transgenic ~12 months old C57BL/6 mice which had received a retro-orbital AAV injection (see above) were used for intracranial Aβ injections. The surgical procedure was identical to the intracranial AAV injection procedure but using exact coordinates for the somatosensory cortex (AP: -1.3 mm; ML: ±2.7 mm; -1.0 mm) and Aβ instead of AAV solution. The left hemisphere was injected with 2 μL of 350 μM oAβ while the right hemisphere was injected with 2 μL of 350 μM scrambled Aβ1-42 (in PBS, Sigma Aldrich). Mice were transcardially perfused with 4% PFA +20 mM NEM 7 days after surgery and subsequently sliced and prepared for imaging.

4.13. Immunofluorescence staining

Mouse brain slices (120 μm thick) obtained following transcardial PFA perfusion were used for immunofluorescence staining. Slices were washed in PBS for 5–10 min after removing CPS. Slices were incubated overnight at 4°C in blocking solution containing 0.1 M PBS, 20% DMSO, 2% Triton-X and 10% Normal Goat Serum (NGS) or Normal Donkey Serum (NDS). After a washing step with PBS, slices were incubated in primary antibody solution containing 0.1 M PBS, 20% DMSO, 2% Triton-X and 2.5% NGS or NDS for 3–5 days at 4°C. The following primary antibodies were used: Iba1, 1:500 (Wako Pure Chemicals, Osaka, Japan); LAMP1, 1:300 (abcam, Cambridge, UK); BACE1 1:300 (abcam); cd11b, 1:500 (BioRad, Hercules, US); ubiquitin 1:50 (Sigma Aldrich, St. Louis, US); P2YR12 1:500 (Anaspec, Fremont, US); Aβ/APP 6E10, 1:250 (Biolegend); Aβ mOC87, 1:500 (abcam); MAP2, 1:1000 (abcam); GFAP, 1:2000 (Thermo Fisher, Waltham, US); Olig2 1:300 (abcam); NOX2 1:500 (Immunological Science, Rome, Italy); myeloperoxidase, 1:50 (abcam); PDGFRβ, 1:100 (Thermo Fisher). Slices were then washed 3–5 times over the course of 4 h in PBS before incubating them in secondary antibody solution for 1–2 days at 4°C containing: 0.1 M PBS, 20%DMSO, 2% Triton-X and 2.5% NGS or NDS. The following conjugated secondary antibodies were used targeted to the respected host species of primary antibodies: Alexa Fluor 546, 568 and 647. Brain slices were then washed 3–5 times in PBS and mounted using FluorSafe™ (Millipore, Massachusetts, US) onto glass slides. For additional staining of amyloid plaque cores slices were stained with 100 μM Methoxy-X04 for 30 min before the last washing steps in 0.1 M PBS, 20%DMSO and 2% Triton-X.

Immunostaining in human brain slices was done as follows: 4 μm thick paraffin-embedded sporadic and familial (PSEN1) AD patient autopsy-derived formalin-fixed prefrontal cortex (PFC) sections were generated by the Vancouver General Hospital pathology core and mounted onto glass slides. PFC sections were deparaffinized with xylene and serially rehydrated in decreasing concentrations of ethanol. Slides were washed 3 times with dH2O and incubated for 10 min in TBS. Antigen retrieval in 10 mM citrate buffer was conducted by incubating slides at ~95 °C in a steamer for 20 min. Slides were allowed to cool for 45 min at room temperature, rinsed 3 times with dH2O, and incubated for 5 min in TBS +0.2% Tween 20 (TBST). An ImmEdge™ PAP pen (Vector Laboratories) was used to draw a hydrophobic barrier on the glass side surrounding the tissue section. Tissue sections were then blocked and permeabilized in 10% fetal bovine serum (Gibco) + 10% normal donkey serum (Sigma-Aldrich) in TBST (blocking buffer) for 2 h at room temperature. Blocking buffer was poured off the slides, and tissue sections were immediately stained with LAMP1 1:500 (BD Biosciences) and Iba1 1:200 (Wako) primary antibodies (diluted in blocking buffer) overnight at room temperature in a hydrated tissue staining rack. Sections were washed 3 times with TBS, and dipped in TBST prior to staining with Alexa Fluor 594 and 647 tagged secondary antibodies (diluted in blocking buffer) for 2 h at room temperature. Tissues were then washed 3 times in TBS, and counterstained for 20 min in a 1:10,000 dilution of 0.2% w/v Thiolflavin S (Sigma Aldrich) in PBS at room temperature. Sections were washed 3 times with TBS and then mounted in VECTASHIELD™ (Vector Laboratories) mounting medium with rectangular cover glass (60 × 24 mm, VWR). Slides were sealed with transparent nail polish and stored at 4 °C until imaging.

4.14. roGFP1 imaging in fixed tissue

To further investigate microglia interactions with oxidized dystrophic neurites and to combine redox imaging with immunohistochemistry we developed a second redox imaging strategy. Although roGFP1 is most typically used for live cell imaging [5,74,77], it was used to image redox levels in Drosophila after fixation with PFA and NEM that acts very rapidly to prevent thiol oxidation thereby preserving roGFP1 redox states [32]. Imaging fixed tissue has two major advantages over live cell imaging: 1.) It would allow immunostainings for proteins of interest and 2.) it avoids the problem of cell degeneration in acute imaging preparations. The latter is of particular importance since any cell damage caused by tissue preparations would likely impact the redox balance of cells.

We tested whether PFA fixation with NEM protocols preserves the roGFP1 redox ratios initially observed during live cell imaging. Mice (non-transgenic (non-tg) or 5xFAD) were intracranially injected with an AAV2/9-CBA-roGFP1 construct at 9–11 months age to induce widespread neuronal cytosolic roGFP1 expression. After 4 weeks mice were either sacrificed for acute brain slice preparations or intracardially perfused with PFA (Fig. S1f).

We first confirmed functional roGFP1 expression in acute brain slices of non-tg animals by live 2-photon imaging. A stepwise bath perfusion of the oxidizing agent diamide (0.1, 0.5 and 2 mM, 10 min each) gradually oxidized cortical neurons while a subsequent application of the reducing agent DTT (5 mM) fully reversed the effect (Fig. S1g). Then we incubated acute brain slices for 10 min in 0.1, 0.5 or 2 mM diamide as well as 5 mM DTT following a 2 min fixation with 4% PFA supplemented with 20 mM N-ethylmaleimide (NEM) at 80°C. NEM binds to thiol groups and prevents the formation of disulfide bonds permanently locking roGFP1 in its oxidation state during the fixation procedure (*32*). Slices were kept for at least 24h in a PBS solution containing 20% DMSO +2% Triton-X + 20 mM NEM to clear the tissue prior to imaging. We hypothesized that the addition of NEM in the fixation procedure will preserve the oxidation state of roGFP1 and that clearing the tissue from lipids might increase the dynamic range of the sensor due to reduced tissue scattering. The PFA fixed acute slices were mounted and imaged under a 2-photon microscope. Indeed, the effect of diamide lead to a very similar change in $R_{ox}F_{GFP}$ while DTT had no significant effect compared to untreated slices (Fig. S1h). However, the dynamic range of roGFP1 in the PFA fixed tissue was superior over the acute preparations (diamide/DTT response; 3.63 ± 0.14 fold (N = 8) vs. 2.78 ± 0.22 fold (N = 5); **p <0.01).

We conclude that our fixation protocol not only allows for functional roGFP1 imaging in PFA fixed brain tissue but also improves the dynamic range of roGFP1 under these conditions.

4.15. Calculation of microglia plaque coverage

Microglia are well known to accumulate and cover the area around amyloid plaques [47] and form a barrier around the highly aggregated plaque core. To test whether the amount of microglia coverage in individual plaques affects local neuronal Ox-stress we used the following approach: roGFP1 expressing 5xFAD brain slices were stained with Methoxy-X04 and immunolabeled for Iba1 and LAMP1. A confocal laser scanning microscope was used to acquire 10 μm z-stacks and maximum z-projections were generated. LAMP1 immunoreactivity appears as a diffuse cloud of DNs around Methoxy-X04 positive plaque cores which was defined as the local plaque area and a mask was generated of the LAMP1 signal (see Fig. 6d). Within this area the Iba1 positive immunoreactivity was also masked and the area calculated. Microglia coverage per plaque was defined as the Iba1 positive area divided by the local LAMP1 positive area in percent.

4.16. Microglia depletion

Microglia depend on CSF1 receptor signaling and blocking this receptor leads to the elimination of microglia of the brain in non-tg as well as 5xFAD mice (*36, 37*). Both non-tg and 5xFAD mice were intracranially injected with AAV at an age of 9 months and were put on a special diet containing 290 mg/kg PLX3397 in the chow. After 8 weeks mice were transcardially perfused and the brains were harvested and sliced for subsequent redox imaging and immunofluorescence staining.

Declaration of competing interest

The authors declare that they have no known competing financial interests or personal relationships that could have appeared to influence the work reported in this paper.

Data availability

Data will be made available on request.

Acknowledgments

This work was supported by a Research Fellowship from the German Research Foundation (DFG) #WE 6264/2-2, the Canadian Institutes of Health Research (CIHR) #FDN148397, The Aune Foundation, the Pacific Alzheimer's Research Foundation and an Alzheimer's Association Research Fellowship #AARF-21-848318. We thank the Mathew Tantama lab for providing plasmids to generate the rogRFP2 construct as well as the Brian Bacskai lab for providing plasmids to generate the roGFP1 construct for this study. The authors thank Rayshad Sharif Gopaul for animal care. B.A.M. was supported by a Canada Research Chair in Neuroscience.

Appendix A. Supplementary data

Supplementary data to this article can be found online at https://doi.org/10.1016/j.redox.2022.102448.

References

[1] E. Tonnies, E. Trushina, Oxidative stress, synaptic dysfunction, and Alzheimer's disease, J Alzheimers Dis 57 (2017) 1105–1121.
[2] Y.-T. Chang, et al., The roles of biomarkers of oxidative stress and Antioxidant in Alzheimer's disease: a systematic review, BioMed Research International 2014 (2014) 1–14.
[3] Z. Chen, C. Zhong, Oxidative stress in Alzheimer's disease, Neurosci. Bull. 30 (2014) 271–281.
[4] A. Fracassi, et al., Oxidative damage and Antioxidant response in frontal cortex of demented and nondemented individuals with Alzheimer's neuropathology, J. Neurosci. 41 (2021) 538–554.
[5] H. Xie, et al., Rapid cell death is preceded by amyloid plaque-mediated oxidative stress, Proc. Natl. Acad. Sci. U. S. A. 110 (2013) 7904–7909.
[6] M. Goedert, Oskar Fischer and the study of dementia, Brain 132 (2008) 1102–1111.
[7] R.D. Terry, H.M. Wiśniewski, In Advances in Behavioral Biology, Springer US, 1972, pp. 89–116.
[8] R.D. Terry, N.K. Gonatas, M. Weiss, Ultrastructural studies in Alzheimer's presenile dementia, Am. J. Pathol. 44 (1964) 269–297.
[9] R.D. Terry, et al., Physical basis of cognitive alterations in Alzheimer's disease: synapse loss is the major correlate of cognitive impairment, Ann. Neurol. 30 (1991) 572–580.
[10] M. Shoji, S. Hirai, H. Yamaguchi, Y. Harigaya, T. Kawarabayashi, Amyloid β-protein precursor accumulates in dystrophic neurites of senile plaques in Alzheimer-type dementia, Brain Res. 512 (1990) 164–168.
[11] P. Cras, et al., Senile plaque neurites in Alzheimer disease accumulate amyloid precursor protein, Proc. Natl. Acad. Sci. USA 88 (1991) 7552–7556.
[12] R. Sanchez-Varo, et al., Abnormal accumulation of autophagic vesicles correlates with axonal and synaptic pathology in young Alzheimer's mice hippocampus, Acta Neuropathol. 123 (2012) 53–70.
[13] P.C. Kandalepas, et al., The Alzheimer's β-secretase BACE1 localizes to normal presynaptic terminals and to dystrophic presynaptic terminals surrounding amyloid plaques, Acta Neuropathol. 126 (2013) 329–352.
[14] K.R. Sadleir, et al., Presynaptic dystrophic neurites surrounding amyloid plaques are sites of microtubule disruption, BACE1 elevation, and increased Aβ generation in Alzheimer's disease, Acta Neuropathol. 132 (2016) 235–256.
[15] L. Blazquez-Llorca, et al., High plasticity of axonal pathology in Alzheimer's disease mouse models, Acta Neuropathologica Communications 5 (2017).
[16] D.V. Hansen, J.E. Hanson, M. Sheng, Microglia in Alzheimer's disease, J. Cell Biol. 217 (2018) 459–472.
[17] H. El Hajj, et al., Ultrastructural evidence of microglial heterogeneity in Alzheimer's disease amyloid pathology, J. Neuroinflammation 16 (2019).
[18] M.T. Heneka, et al., Neuroinflammation in Alzheimer's disease, Lancet Neurol. 14 (2015) 388–405.
[19] F. Leng, P. Edison, Neuroinflammation and microglial activation in Alzheimer disease: where do we go from here? Nat. Rev. Neurol. 17 (2021) 157–172.
[20] K.I. Mosher, T. Wyss-Coray, Microglial dysfunction in brain aging and Alzheimer's disease, Biochem. Pharmacol. 88 (2014) 594–604.
[21] J.J. Tang, et al., Cognitive enhancement and neuroprotective effects of OABL, a sesquiterpene lactone in 5xFAD Alzheimer's disease mice model, Redox Biol. 50 (2022), 102229.
[22] S. Radhakrishnan, et al., Neuron activity dependent redox compartmentation revealed with a second generation red-shifted ratiometric sensor, ACS Chem. Neurosci. 11 (2020) 2666–2678.
[23] B.L. Wilkinson, G.E. Landreth, The microglial NADPH oxidase complex as a source of oxidative stress in Alzheimer's disease, J. Neuroinflammation 3 (2006) 30.
[24] D.S.A. Simpson, P.L. Oliver, ROS generation in microglia: understanding oxidative stress and inflammation in neurodegenerative disease, Antioxidants 9 (2020).
[25] C. Cheignon, et al., Oxidative stress and the amyloid beta peptide in Alzheimer's disease, Redox Biol. 14 (2018) 450–464.
[26] A. Misrani, S. Tabassum, L. Yang, Mitochondrial dysfunction and oxidative stress in Alzheimer's disease, Front. Aging Neurosci. 13 (2021), 617588.
[27] M.G. Sharoar, S. Palko, Y. Ge, T.C. Saido, R. Yan, Accumulation of saposin in dystrophic neurites is linked to impaired lysosomal functions in Alzheimer's disease brains, Mol. Neurodegener. 16 (2021) 45.
[28] S. Gowrishankar, et al., Massive accumulation of luminal protease-deficient axonal lysosomes at Alzheimer's disease amyloid plaques, Proc. Natl. Acad. Sci. USA 112 (2015) E3699–E3708.
[29] S. Kugler, E. Kilic, M. Bahr, Human synapsin 1 gene promoter confers highly neuron-specific long-term transgene expression from an adenoviral vector in the adult rat brain depending on the transduced area, Gene Ther. 10 (2003) 337–347.
[30] G. Di Guardo, Lipofuscin, lipofuscin-like pigments and autofluorescence, Eur. J. Histochem. 59 (2015) 2485.
[31] Y. Mochizuki, M.K. Park, T. Mori, S. Kawashima, The difference in autofluorescence features of lipofuscin between brain and adrenal, Zool. Sci. (Tokyo) 12 (1995) 283–288.
[32] Simone C. Albrecht, Ana G. Barata, J. Großhans, Aurelio A. Teleman, Tobias P. Dick, In vivo mapping of hydrogen peroxide and oxidized glutathione reveals chemical and regional specificity of redox homeostasis, Cell Metabol. 14 (2011) 819–829.
[33] Y. Fujikawa, et al., Mouse redox histology using genetically encoded probes, Sci. Signal. 9 (2016) rs1.
[34] H. Oakley, et al., Intraneuronal beta-amyloid aggregates, neurodegeneration, and neuron loss in transgenic mice with five familial Alzheimer's disease mutations: potential factors in amyloid Plaque Formation, J. Neurosci. 26 (2006) 10129–10140.
[35] L.P. Bernier, et al., Nanoscale surveillance of the brain by microglia via cAMP-regulated filopodia, Cell Rep. 27 (2019) 2895–2908 e2894.
[36] E.E. Spangenberg, et al., Eliminating microglia in Alzheimer's mice prevents neuronal loss without modulating amyloid-β pathology, Brain 139 (2016) 1265–1281.
[37] R.A. Rice, et al., Elimination of microglia improves functional outcomes following extensive neuronal loss in the Hippocampus, J. Neurosci. 35 (2015) 9977–9989.
[38] E.M. York, N.L. Weilinger, J.M. LeDue, B.A. MacVicar, Green fluorescent protein emission obscures metabolic fluorescent lifetime imaging of NAD(P)H, Biomed. Opt Express 10 (2019) 4381–4394.

[39] B. Das, R. Yan, Role of BACE1 in Alzheimer's synaptic function, Transl. Neurodegener. 6 (2017).
[40] D.A. Butterfield, A.M. Swomley, R. Sultana, Amyloid β-peptide (1–42)-induced oxidative stress in Alzheimer disease: importance in disease pathogenesis and progression, Antioxidants Redox Signal. 19 (2013) 823–835.
[41] F. Wang, R. Gómez-Sintes, P. Boya, Lysosomal membrane permeabilization and cell death, Traffic 19 (2018) 918–931.
[42] C. Papadopoulos, H. Meyer, Detection and clearance of damaged lysosomes by the endo-lysosomal damage response and lysophagy, Curr. Biol. 27 (2017) R1330–R1341.
[43] C.D. Austin, et al., Oxidizing potential of endosomes and lysosomes limits intracellular cleavage of disulfide-based antibody-drug conjugates, Proc. Natl. Acad. Sci. USA 102 (2005) 17987–17992.
[44] M.L. Block, NADPH oxidase as a therapeutic target in Alzheimer's disease, BMC Neurosci. 9 (2008) S8.
[45] S. Gellhaar, D. Sunnemark, H. Eriksson, L. Olson, D. Galter, Myeloperoxidase-immunoreactive cells are significantly increased in brain areas affected by neurodegeneration in Parkinson's and Alzheimer's disease, Cell Tissue Res. 369 (2017) 445–454.
[46] P.S. Green, et al., Neuronal expression of myeloperoxidase is increased in Alzheimer's disease, J. Neurochem. 90 (2004) 724–733.
[47] C. Condello, P. Yuan, A. Schain, J. Grutzendler, Microglia constitute a barrier that prevents neurotoxic protofibrillar Abeta42 hotspots around plaques, Nat. Commun. 6 (2015) 6176.
[48] W.A. Eimer, R. Vassar, Neuron loss in the 5XFAD mouse model of Alzheimer's disease correlates with intraneuronal Aβ42 accumulation and Caspase-3 activation, Mol. Neurodegener. 8 (2013) 2.
[49] S. Jung, et al., Analysis of fractalkine receptor CX(3)CR1 function by targeted deletion and green fluorescent protein reporter gene insertion, Mol. Cell Biol. 20 (2000) 4106–4114.
[50] R.T. Sasmono, et al., A macrophage colony-stimulating factor receptor-green fluorescent protein transgene is expressed throughout the mononuclear phagocyte system of the mouse, Blood 101 (2003) 1155–1163.
[51] C.V. Piattoni, et al., New red-shifted fluorescent biosensor for monitoring intracellular redox changes, Free Radic. Biol. Med. 134 (2019) 545–554.
[52] A.G. Shokhina, et al., Red fluorescent redox-sensitive biosensor Grx1-roCherry, Redox Biol. 21 (2019), 101071.
[53] Y. Fan, Z. Chen, H.W. Ai, Monitoring redox dynamics in living cells with a redox-sensitive red fluorescent protein, Anal. Chem. 87 (2015) 2802–2810.
[54] S. Norcross, et al., Extending roGFP emission via förster-type resonance energy transfer relay enables simultaneous dual compartment ratiometric redox imaging in live cells, ACS Sens. 2 (2017) 1721–1729.
[55] E. Spangenberg, et al., Sustained microglial depletion with CSF1R inhibitor impairs parenchymal plaque development in an Alzheimer's disease model, Nat. Commun. 10 (2019) 3758.
[56] M.S. Unger, P. Schernthaner, J. Marschallinger, H. Mrowetz, L. Aigner, Microglia prevent peripheral immune cell invasion and promote an anti-inflammatory environment in the brain of APP-PS1 transgenic mice, J. Neuroinflammation 15 (2018) 274.
[57] J.H. Zhang, A. Ferrante, A.P. Arrigo, J.M. Dayer, Neutrophil stimulation and priming by direct contact with activated human T lymphocytes, J. Immunol. 148 (1992) 177–181.
[58] T. Jonsson, et al., Variant of TREM2 associated with the risk of Alzheimer's disease, N. Engl. J. Med. 368 (2013) 107–116.
[59] R. Guerreiro, et al., TREM2 variants in Alzheimer's disease, N. Engl. J. Med. 368 (2013) 117–127.
[60] P. Yuan, et al., TREM2 haplodeficiency in mice and humans impairs the microglia barrier function leading to decreased amyloid compaction and severe axonal dystrophy, Neuron 90 (2016) 724–739.
[61] C. Condello, P. Yuan, J. Grutzendler, Microglia-Mediated neuroprotection, TREM2, and Alzheimer's disease: evidence from optical imaging, Biol. Psychiatr. 83 (2018) 377–387.
[62] Z. Zhou, et al., Crowded cell-like environment accelerates the nucleation step of amyloidogenic protein misfolding, J. Biol. Chem. 284 (2009) 30148–30158.
[63] S. Gowrishankar, Y. Wu, S.M. Ferguson, Impaired JIP3-dependent axonal lysosome transport promotes amyloid plaque pathology, J. Cell Biol. 216 (2017) 3291–3305.
[64] M.G. Sharoar, X. Hu, X.-M. Ma, X. Zhu, R. Yan, Sequential formation of different layers of dystrophic neurites in Alzheimer's brains, Mol. Psychiatr. 24 (2019) 1369–1382.
[65] J.H. Lee, et al., Faulty autolysosome acidification in Alzheimer's disease mouse models induces autophagic build-up of Abeta in neurons, yielding senile plaques, Nat. Neurosci. 25 (2022) 688–701.
[66] P. Boya, Lysosomal function and dysfunction: mechanism and disease, Antioxidants Redox Signal. 17 (2012) 766–774.
[67] D. Butler, B.A. Bahr, Oxidative stress and lysosomes: CNS-related consequences and implications for lysosomal enhancement strategies and induction of autophagy, Antioxidants Redox Signal. 8 (2006) 185–196.
[68] T. Mizuno, The biphasic role of microglia in Alzheimer's disease, Int. J. Alzheimer's Dis. 2012 (2012), 737846.
[69] A.L. Hemonnot, J. Hua, L. Ulmann, H. Hirbec, Microglia in Alzheimer disease: well-known targets and new opportunities, Front. Aging Neurosci. 11 (2019) 233.
[70] B. Zhang, et al., The microtubule-stabilizing agent, epothilone D, reduces axonal dysfunction, neurotoxicity, cognitive deficits, and Alzheimer-like pathology in an interventional study with aged tau transgenic mice, J. Neurosci. 32 (2012) 3601–3611.
[71] J.J. Fernandez-Valenzuela, et al., Enhancing microtubule stabilization rescues cognitive deficits and ameliorates pathological phenotype in an amyloidogenic Alzheimer's disease model, Sci. Rep. 10 (2020), 14776.
[72] A.M. Floden, S. Li, C.K. Combs, Beta-amyloid-stimulated microglia induce neuron death via synergistic stimulation of tumor necrosis factor alpha and NMDA receptors, J. Neurosci. 25 (2005) 2566–2575.
[73] T. Yardeni, M. Eckhaus, H.D. Morris, M. Huizing, S. Hoogstraten-Miller, Retro-orbital injections in mice, Lab Anim (NY) 40 (2011) 155–160.
[74] C.T. Dooley, et al., Imaging dynamic redox changes in mammalian cells with green fluorescent protein indicators, J. Biol. Chem. 279 (2004) 22284–22293.
[75] G.T. Hanson, et al., Investigating mitochondrial redox potential with redox-sensitive green fluorescent protein indicators, J. Biol. Chem. 279 (2004) 13044–13053.
[76] Y.Y. Jean, J. Baleriola, M. Fa, U. Hengst, C.M. Troy, Stereotaxic infusion of oligomeric amyloid-beta into the mouse Hippocampus, J Vis Exp (2015), e52805.
[77] K.A. Lukyanov, V.V. Belousov, Genetically encoded fluorescent redox sensors, Biochim. Biophys. Acta Gen. Subj. 1840 (2014) 745–756.
[78] D.G. Walker, et al., Patterns of expression of purinergic receptor P2RY12, a putative marker for non-activated microglia, in aged and Alzheimer's disease brains, Int. J. Mol. Sci. 21 (2020).